LUND UNIVERSITY

Doping of Semiconductor Nanowires

Wallentin, Jesper

2012

Link to publication

Citation for published version (APA):
Wallentin, J. (2012). *Doping of Semiconductor Nanowires*. Lund University.

Total number of authors:
1

General rights
Unless other specific re-use rights are stated the following general rights apply:
Copyright and moral rights for the publications made accessible in the public portal are retained by the authors and/or other copyright owners and it is a condition of accessing publications that users recognise and abide by the legal requirements associated with these rights.
• Users may download and print one copy of any publication from the public portal for the purpose of private study or research.
• You may not further distribute the material or use it for any profit-making activity or commercial gain
• You may freely distribute the URL identifying the publication in the public portal

Read more about Creative commons licenses: https://creativecommons.org/licenses/

Take down policy
If you believe that this document breaches copyright please contact us providing details, and we will remove access to the work immediately and investigate your claim.

LUND UNIVERSITY

PO Box 117
221 00 Lund
+46 46-222 00 00

Doping of semiconductor nanowires

Jesper Wallentin

Doctoral thesis
2013

LUND
UNIVERSITY

Division of Solid State Physics
Department of Physics
Lund University

Academic Dissertation which, by due permission of the Faculty of Engineering at Lund University, will be publicly defended on Friday, January 18th, 2013 at 10:15 in Rydbergsalen, Sölvegatan 14, Lund, for the degree of Doctor of Philosophy in Engineering.

Doping of semiconductor nanowires

Jesper Wallentin

Doctoral thesis
2013

LUND UNIVERSITY

Division of Solid State Physics
Department of Physics
Lund University

Copyright © Jesper Wallentin 2012

Division of Solid State Physics
Department of Physics
Lund University
221 00 Lund
Sweden

ISBN 978-91-7473-439-3

Printed in Sweden by Media-Tryck, Lund University
Lund 2012

Till Verena,

Sonja och Eskil

Table of Content

Abstract **9**

Populärvetenskaplig sammanfattning **11**

List of papers **15**

1 Introduction **19**

2 Solar cells **23**

2.1 Sunlight 23
2.2 The p-n junction 25
2.3 Current-voltage characteristics 26
2.4 Efficiency limitations 28
2.5 Multijunction solar cells 29
2.6 Nanowire solar cells 32

3 Nanowire growth **35**

3.1 Crystal growth 35
3.2 Nucleation theory 36
3.3 Mass transport 41
3.3.1 Transport in carrier gas. 41
3.3.2 Pyrolysis 42
3.3.3 Surface diffusion on substrate 42
3.3.4 Surface diffusion on NW side facets 43
3.3.5 Incorporation in seed particle 43
3.3.6 Parasitic processes 43
3.4 Polytypism 44
3.5 Fabrication of nanowire solar cells 46

4 Dopant incorporation **47**
4.1 Axial growth 48
4.2 Incorporation in radial growth 50
4.3 Carrier generation 50
4.4 Summary 52

5 Effects of *in situ* doping on nanowire growth **53**
5.1 Growth rate 53
5.2 Growth instability 55
5.3 Structural effects 56
5.4 Compositional effects 57
5.5 Summary 58

6 Nanowire doping measurements **59**
6.1 Electrical methods 59
6.2 Optical methods 62
6.3 Electron beam and X-ray methods 63
6.4 Mass spectrometric methods 64
6.5 Scanning probe methods 65

7 Conclusions **67**

References **69**

Acknowledgements **81**

Abstract

In this thesis, *in situ* doping during growth of III-V semiconductor nanowires, primarily for photovoltaic applications, is investigated. The nanowires were grown by metalorganic vapor phase epitaxy (MOVPE), with gold seed particles. After growth the nanowires were characterized using various techniques, including photoluminescence, transmission electron microscopy and electrical measurements of contacted nanowires. Different III-V materials were studed, both binary materials such as InP and GaAs, and ternary materials such as $Ga_xIn_{1-x}P$. To achieve p- and n-doping, different precursors were employed.

The results show that successful p- and n-doping can be achieved in many materials. The *in situ* doping is shown to affect the nanowire growth strongly, but differently depending on the combination of material and dopant. The main effects are related to the growth rate and the crystal structure. It is shown that the n-dopant H_2S increases the growth rate and induces wurtzite crystal structure in InP nanowires, while the p-dopant DEZn gives an unchanged growth rate with zinc blende crystal structure.

High doping and sharp doping profiles are demonstrated with interband tunneling in Esaki tunnel diodes. Finally, *in situ* doping is used to create p-i-n doped InP nanowire arrays which are processed into solar cells with 13.8% efficiency.

Populärvetenskaplig sammanfattning

Vi människor konsumerar en ständigt ökande mängd elektrisk energi, som till största delen produceras av ändligt tillgängliga material som kol, gas, olja och uran. Elproduktionen har många skadliga bieffekter, som till exempel utsläpp av växthusgasen koldioxid vid förbränning av kol, gas och olja. Solceller omvandlar istället solens ljus direkt till elektricitet. Processen sker helt utan utsläpp och har inga rörliga mekaniska delar som kan slitas. Råvaran, solljus, finns relativt jämnt fördelad över hela jorden och behöver inte transporteras. Tack vare dessa fördelar blir elproduktion med solceller allt populärare, och är globalt sett ungefär lika betydelsefull som vindkraft.

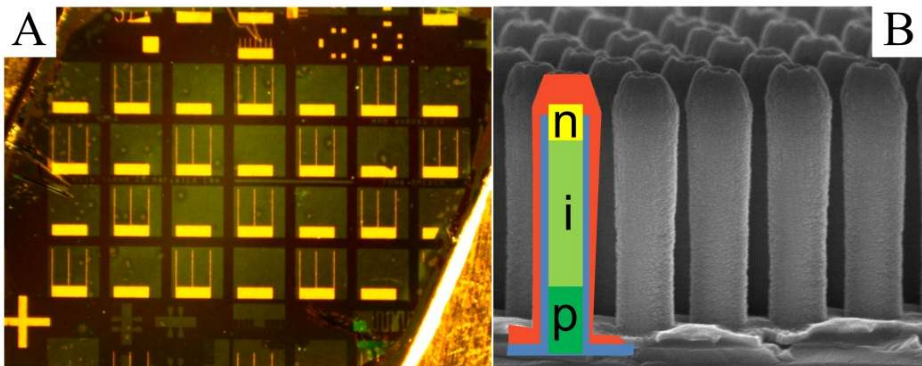

Figur 1. Solceller baserade på nanotrådar. *A) Ljusmikroskopbild på ett prov med 26 solceller. Varje solcell mäter 1x1 millimeter, och hela provet mäter ungefär 1x1 centimeter. B) Elektronmikroskopbild av nanotrådar från en solcell. Varje nanotråd är cirka 1.5 mikrometer (µm, tusendels millimeter) lång, och cirka 0.2 mikrometer i diameter. Som jämförelse är ett hårstrå 50 mikrometer tjockt.*

I den här avhandlingen har dopning av III-V nanotrådar undersökts, med syftet att göra nanotrådsbaserade solceller. Olika sorters III-V material och dopämnen har undersökts. Resultaten visar att det är möjligt att dopa flertalet av de undersökta materialen. Med hjälp av dopningen har nanotrådsbaserade solceller med en verkningsgrad på 13.8% tillverkats. Det är den högsta rapporterade verkningsgraden för nanostrukturerade solceller, och bara lite sämre än den genomsnittliga verkningsgraden på 15% för kommersiella kiselsolceller. Eftersom

nanotrådssolcellerna bara har utvecklats under några år, jämfört med flera decennier för kiselsolcellerna, så är detta ett lovande resultat.

En solcells förmåga att omvandla solljus till elektricitet kallas för verkningsgrad. Idag baseras de flesta solceller på grundämnet kisel, vilket är samma material som är basen för elektroniken i alla datorer. Detta material ger en medelmåttig verkningsgrad för ett medelmåttigt pris. För att göra solceller ännu mer användningsbara utvecklar många forskare och företag nya sorters solceller, som är billigare eller bättre än kiselceller. De mest effektiva solcellerna görs av så kallade III-V (”tre-fem”) material, som kan ge ungefär dubbelt så mycket eleffekt som kiselceller. Tyvärr är III-V material dyra, vilket gör dessa solceller olönsamma för de flesta tillämpningar.

Ett möjligt sätt att sänka kostnaderna är att göra III-V materialet i form av små, avlånga kristaller som kallas nanotrådar. Dessa nanotrådar är ungefär en tusendel så tjocka som ett hårstrå, vilket betyder att deras diameter är ungefär samma som ljusets våglängd. Mängden III-V material som används kan då minskas på två sätt. Dels kan man använda ett annat, billigare material som bärande substrat, dels behöver man bara täcka ungefär en tiondel av ytan. Nanotrådarna fungerar som små antenner som effektivt fångar in solljuset.

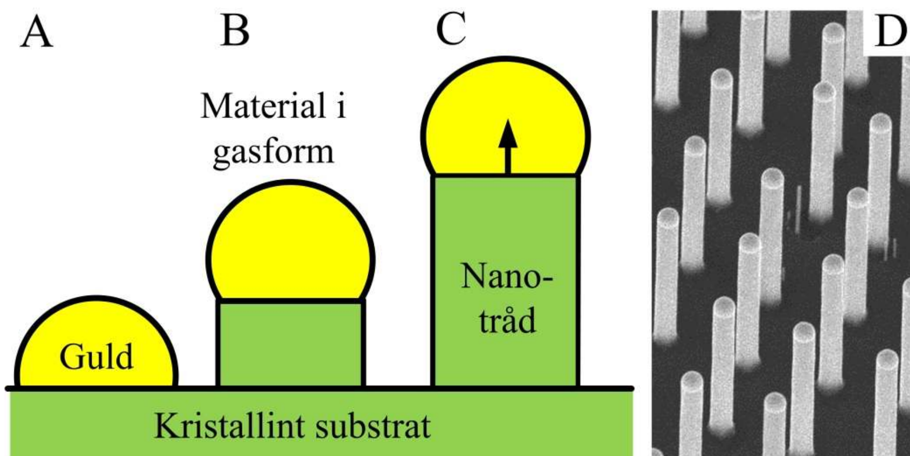

Figur 2 Nanotrådsväxt *A) Guld läggs på ett kristallint substrat. B) Material i gasform tillförs. Kristallen växer då vid gränsen mellan guldpartikeln och substratet. C) Guldpartikeln lyfts upp av den framväxande nanotråden. D) Elektronmikroskopbild av färdiga nanotrådar, snett uppifrån. Varje nanotråd är drygt en mikrometer lång.*

I en solcell absorberas ljusenergin av elektroner, som tvingas i en bestämd riktning vilket skapar en elektrisk ström. För att göra detta används så kallad dopning,

vilket innebär att man stoppar in kontrollerade mängder av speciella föroreningar i den annars mycket rena kristallen. Med n-dopning skapar man ett överskott av elektroner, och med p-dopning skapar man ett underskott. Kombinerar man ett p-dopat och ett n-dopat område får man en p-n övergång, som också kallas en diod. Det är i övergången mellan p-dopning och n-dopning som elektronerna tvingas i en speciell riktning, nämligen mot den n-dopade sidan. För att nanotrådarna ska fungera som solceller måste därför dessa kunna både n-dopas och p-dopas, vilket är temat för denna avhandling.

Forskningen som beskrivs i avhandlingen visar att dopning påverkar kristallväxten på flera sätt. Vissa dopämnen ökar växthastigheten, medan vissa ändrar kristallens struktur. I de flesta fall är dock dopningen framgångsrik, på så sätt att det går att få avsedd p- eller n-dopning. Genom att kombinera p- och n-dopning i samma nanotråd skapas en p-n övergång, det vill säga en diod. När denna ansluts till en elektrisk krets med hjälp av ledande kontakter så skapas en solcell.

List of papers

I. J. Wallentin, J. M. Persson, J. B. Wagner, L. Samuelson, K. Deppert, M. T. Borgström, *High-Performance Single Nanowire Tunnel Diodes*. Nano Letters, 2010, 10, 974

I grew the nanowires, performed the processing and electrical measurements, and was responsible for writing the paper.

II. J. Wallentin, M. Ek, L. R. Wallenberg, L. Samuelson, K. Deppert, M. T. Borgström, *Changes in Contact Angle of Seed Particle Correlated with Increased Zincblende Formation in Doped InP Nanowires*. Nano Letters, 2010, 10, 4807

I grew the nanowires, performed the SEM measurements, developed the theoretical model, and was responsible for writing the paper.

III. J. Wallentin, M. E. Messing, E. Trygg, L. Samuelson, K. Deppert, M. T. Borgström, *Growth of doped InAsyP1-y nanowires with InP shells*. Journal of Crystal Growth, 2011, 331, 8

I grew the nanowires, performed some of the measurements and wrote parts of the paper.

IV. J. Wallentin, K. Mergenthaler, M. Ek, L. R. Wallenberg, L. Samuelson, K. Deppert, M. E. Pistol, M. T. Borgström, *Probing the Wurtzite Conduction Band Structure Using State Filling in Highly Doped InP Nanowires*. Nano Letters, 2011, 11, 2286

I grew the nanowires, performed some of the measurements, and was responsible for writing the paper.

V. M. T. Borgström, J. Wallentin, M. Heurlin, S. Fält, P. Wickert, J. Leene, M. H. Magnusson, K. Deppert, L. Samuelson, *Nanowires With Promise for Photovoltaics*. IEEE Journal of Selected Topics in Quantum Electronics, 2011, 17, 1050

I performed some of the experimental work, and wrote parts of the paper.

VI. J. Wallentin, M. T. Borgström, *Doping of semiconductor nanowires*. Journal of Materials Research, 2011, 26, 2142

I was responsible for writing the paper.

VII. J. Wallentin, P. Wickert, M. Ek, A. Gustafsson, L. R. Wallenberg, M. H. Magnusson, L. Samuelson, K. Deppert, M. T. Borgström, *Degenerate p-doping of InP nanowires for large area tunnel diodes*. Applied Physics Letters, 2011, 99, 253105

I grew the nanowires, performed some of the processing and electrical measurements, and was responsible for writing the paper.

VIII. J. Wallentin, M. Ek, L. R. Wallenberg, L. Samuelson, M. T. Borgström, *Electron Trapping in InP Nanowire FETs with Stacking Faults*. Nano Letters, 2011, 12, 151

I grew the nanowires, performed the processing and electrical measurements, developed the theoretical model, and was responsible for writing the paper.

IX. J. Wallentin, L. B. Poncela, A. M. Jansson, K. Mergenthaler, M. Ek, D. Jacobsson, L. R. Wallenberg, K. Deppert, L. Samuelson, D. Hessman, M. T. Borgström, *Single GaInP nanowire p-i-n junctions near the direct to indirect bandgap crossover point*. Applied Physics Letters, 2012, 100, 251103

I grew the nanowires, performed some of the measurements, and was responsible for writing the paper.

X. J. Wallentin, N. Anttu, D. Asoli, M. Huffman, I. Åberg, M. H. Magnusson, G. Siefer, P. Fuss-Kailuweit, F. Dimroth, B. Witzigmann, H. Q. Xu, L. Samuelson, K. Deppert, M. T. Borgström, *InP nanowire array solar cells achieving 13.8% efficiency by exceeding the ray-optics-limit*. Submitted, 2012

I grew the nanowires and was responsible for writing the paper.

Papers not included

The following papers are not included since the content is out of the scope of this thesis:

1. M. T. Borgström, J. Wallentin, J. Trägårdh, P. Ramvall, M. Ek, L. R. Wallenberg, L. Samuelson, K. Deppert, *In Situ Etching for Total Control Over Axial and Radial Nanowire Growth*. Nano Research, 2010, 3, 264
2. M. T. Borgström, K. Mergenthaler, M. E. Messing, U. Håkanson, J. Wallentin, L. Samuelson, M.-E. Pistol, *Fabrication and characterization of AlP-GaP core-shell nanowires*. Journal of Crystal Growth, 2011, 324, 290
3. M. T. Borgström, J. Wallentin, K. Kawaguchi, L. Samuelson, K. Deppert, *Dynamics of extremely anisotropic etching of InP nanowires by HCl*. Chemical Physics Letters, 2011, 502, 222
4. K. Storm, G. Nylund, M. Borgström, J. Wallentin, C. Fasth, C. Thelander, L. Samuelson, *Gate-Induced Fermi Level Tuning in InP Nanowires at Efficiency Close to the Thermal Limit*. Nano Letters, 2011, 11, 1127
5. C. Borschel, M. E. Messing, M. T. Borgström, W. Paschoal, J. Wallentin, S. Kumar, K. Mergenthaler, K. Deppert, C. M. Canali, H. Pettersson, L. Samuelson, C. Ronning, *A New Route toward Semiconductor Nanospintronics: Highly Mn-Doped GaAs Nanowires Realized by Ion-Implantation under Dynamic Annealing Conditions*. Nano Letters, 2011, 11, 3935
6. K. Storm, G. Nylund, M. Borgström, J. Wallentin, C. Fasth, C. Thelander, L. Samuelson, in *Creating dynamic nanowire devices using wrapped gates*. in *Device Research Conference (DRC), 2011 69th Annual*. (2011) 105

7. D. Kriegner, E. Wintersberger, K. Kawaguchi, J. Wallentin, M. T. Borgström, J. Stangl, *Unit cell parameters of wurtzite InP nanowires determined by x-ray diffraction*. Nanotechnology, 2011, 22, 425704
8. M. Hjort, J. Wallentin, R. Timm, A. A. Zakharov, J. N. Andersen, L. Samuelson, M. T. Borgström, A. Mikkelsen, *Doping profile of InP nanowires directly imaged by photoemission electron microscopy*. Applied Physics Letters, 2011, 99, 233113
9. K. Storm, G. Nylund, M. Borgström, J. Wallentin, C. Fasth, C. Thelander, L. Samuelson, *Dual-gate induced InP nanowire diode*. AIP Conference Proceedings, 2011, 1399, 279
10. F. Boxberg, N. Sondergard, H. Q. Xu, J. Wallentin, A. Jin, E. Trygg, M. T. Borgström, *Photovoltaics with piezoelectric core-shell nanowires*. AIP Conference Proceedings, 2011, 1399, 469
11. H. Pettersson, I. Zubritskaya, N. T. Nghia, J. Wallentin, M. T. Borgström, K. Storm, L. Landin, P. Wickert, F. Capasso, L. Samuelson, *Electrical and optical properties of InP nanowire ensemble p+ – i – n+ photodetectors*. Nanotechnology, 2012, 23, 135201
12. B. Ganjipour, J. Wallentin, M. T. Borgström, L. Samuelson, C. Thelander, *Tunnel Field-Effect Transistors Based on InP-GaAs Heterostructure Nanowires*. ACS Nano, 2012, 6, 3109
13. D. Jacobsson, J. M. Persson, D. Kriegner, T. Etzelstorfer, J. Wallentin, J. B. Wagner, J. Stangl, L. Samuelson, K. Deppert, M. T. Borgström, *Particle-assisted GaxIn1-xP nanowire growth for designed band gap structures*. Nanotechnology, 2012, 23, 245601
14. M. Hjort, J. Wallentin, R. Timm, A. A. Zakharov, U. Håkanson, J. N. Andersen, E. Lundgren, L. Samuelson, M. T. Borgström, and A. Mikkelsen, *Surface Chemistry, Structure, and Electronic Properties from Microns to the Atomic Scale of Axially Doped Semiconductor Nanowires.* ACS Nano, 2012, 6 (11), 9679

1 Introduction

The human civilization consumes an increasing amount of electrical power. In 2011, the consumption was over 20 000 TWh [1], up from about 8 000 TWh in 1980. Less than 20% of the electricity was produced with renewable methods, but instead used energy from coal, oil, gas and uranium. The growth in usage of these finite resources will eventually stop.

Although there are finite amounts of energy stored in the form of fossil fuels, earth is not a closed system. The sun is a powerful fusion reactor which emits 3.9×10^{26} W of radiation [2]. Since the sun is about 1.5×10^{11} m away only about 1.2×10^{17} W reaches earth, meaning that 10 minutes of power equals the human population's yearly energy consumption [3]. Clearly, there is an enormous potential in collecting and transforming this solar irradiation into electrical power.

Method	Power (W)
Power of the sun [2]	3.9×10^{26}
Solar irradiation on earth [3]	1.2×10^{17}
Power used for photosynthesis [3]	1.3×10^{14}
Global electrical power production, average [1]	2.3×10^{12}
Photovoltaic power generation, peak (end 2011) [4]	6×10^{10}

Figure 1.1 Comparison of various power sources and conversion methods.

Photovoltaics (PV) is a method of converting sunlight into electrical power, which has seen strong growth the last decade. At the end of 2011, the installed peak power of PV systems was about 6×10^{10} W (60 GW), twice as much as one year earlier [4]. About 51 GW of this peak power was connected during the period 2000-2011, which can be compared with the installations of wind power, 84 GW, gas, 116 GW, and nuclear, which decreased by 14 GW [5] during the same period. In Europe, PV accounted for about 2% of the total electrical energy production in 2011. Despite this strong growth, less than one millionth of the sunlight hitting earth is converted into electricity by PV.

The growth in PV installations has been primarily driven by reduced costs, not by improved performance. The last 10 years has seen an improvement in average produced PV module efficiency, based on crystalline silicon (Si), from 12% to 15% [4]. During the same time, the average price dropped by about 70%.

PV devices normally rely on a p-n junction in a semiconductor, as will be described more thoroughly in the next chapter. Most of the PV devices which are currently installed are based on Si. Since Si is the base for the huge microelectronics industry, there are production methods to create Si of extremely high purity and crystal quality. However, Si is an indirect-bandgap material which means that relatively thick solar cells are needed.

Method	**Conversion efficiency**
Photosynthesis (photons to biomass) [3]	0.3%
Average production Si PV module [4]	15%
Record Si PV cell [6]	25%
Record III-V single junction cell (GaAs) [6]	28.8%
Record III-V multijunction, 1 sun [6]	37.5%
Record III-V multijunction, 418 suns concentration [6]	43.5%

Figure 1.2 Efficiencies of various power conversion methods.

Most semiconductors based on III-V materials, such as indium phosphide (InP) and gallium arsenide (GaAs), have direct bandgaps which gives much higher probability for absorption. These materials form the active layers of the lasers and detectors in fiber optical telecommunications systems, and are also used in the highest-efficiency solar cells. Unfortunately, the production costs for III-V materials are much higher than those for Si. This is a minor problem for millimeter-sized telecommunications components, but it is a major problem for meter-sized solar cells. Therefore, III-V solar cells have mainly been deployed in space applications.

Although the active layer in III-V cells is only a few microns thick, the samples are usually hundreds of microns thick for mechanical stability. One way of combining the low cost of Si with the high performance of III-Vs, is to directly grow active III-V layers on Si substrates. Due to the small lattice constant of Si, however, thin film growth of InP or GaAs on Si substrates leads to defects

forming at the heterointerface. These defects propagate into the active device regions and lead to poor device performance.

A few years ago it was shown that III-V nanowires (NW) can be grown on Si substrates [7]. Not only the lattice-matched GaP can be grown, but also highly strained materials such as GaAs and InP [7]. Importantly, strain-induced defects tend to terminate at the heterointerface, away from the active region [8]. Materials with very large lattice mismatch can be combined in NWs, which could allow multijunction cells with a better bandgap combination to match the solar spectrum. Therefore, many researchers are now investigating NW-based PV [9-13]. Reviews of NW-based PV can be found in ref [11], paper V and references therein.

As described in the next chapter, solar cells are based on semiconductors which have been doped to form a p-n junction. In order to create NW-based solar cells, a good control of doping is necessary. The main goal of this thesis has been to investigate *in situ* doping of III-V NWs for PV applications.

This thesis is structured as follows. First, an introduction to solar cells is made, followed by a description of NW growth. Then, the incorporation during *in situ* doping is discussed, followed by a discussion of effects of doping on NW growth. Finally, a review of doping measurements for NWs is presented.

2 Solar cells

Photovoltaic devices rely on the creation of electron-hole pairs from sunlight, separation of the electrons and holes, and collection of the carriers at contacts. The separation of electrons and holes can be done in several ways, but the vast majority of PV devices rely on the built-in electric field of a p-n junction. This is the type of device which will be discussed in this chapter.

2.1 Sunlight

The sun is a giant fusion reactor, driven primarily by the fusion of four hydrogen ions (protons) into one helium nucleus [2]. For each complete reaction, which occurs about 10^{38} times per second, a net energy of 26.7 MeV is released. The power from the fusion reactions is primarily released as high-energy gamma rays, which are re-absorbed by the plasma in the sun and re-emitted at a slightly lower energy. After thousands of years, the light reaches the surface of the sun and is emitted into space. Since the sun's surface is much cooler than the core, the sun emits light similar to an ideal black-body radiator at about 5500 °C (Fig. 2.1), although the core of the sun has a temperature of about 15 million °C. The human eye is sensitive in the range 400 nm (3 eV) to 750 nm (1.6 eV), and a large part of the solar irradiation is in the invisible near-infrared.

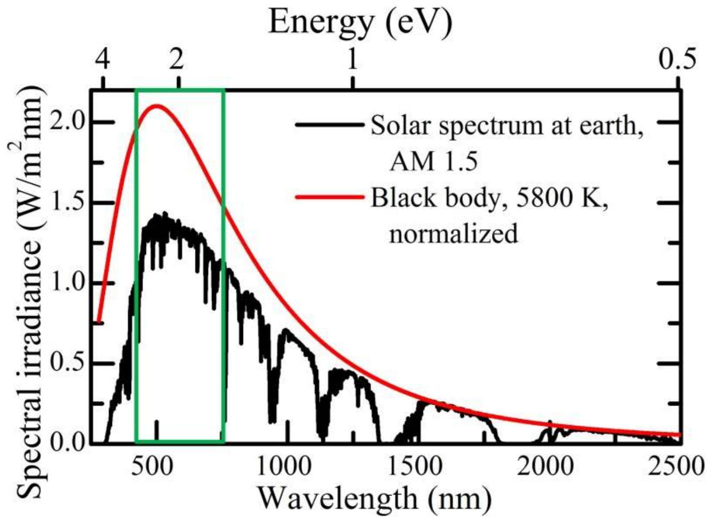

Figure 2.1 Solar spectrum. *The spectrum of solar irradiation at earth ground level (AM1.5), and the normalized spectrum of a 5800 K (5527 °C) black body radiator. The visible region, which ranges from 400 nm to 750 nm, has been indicated with a green box.*

Before the sunlight hits the surface of the earth, parts of the radiation are absorbed and scattered by molecules in the atmosphere, and this absorption shows up as dips in the solar spectrum at earth (Fig. 2.1). The amount of light which is lost this way depends on how much air mass the light has to pass through, which in turn depends on the position of the sun in the sky. When the sun is close to the horizon, more light is scattered and absorbed. These effects are stronger for short-wavelength (blue) light, which explains why the sun appears more red at dawn.

To be able to compare the performance of different PV systems, it is however critical to use a standardized spectrum. The so-called air mass coefficient, AM, is used to define how much air the sunlight has passed through. AM0 is the spectrum outside of the atmosphere, and this spectrum is used to compare PV systems for space applications. AM1 is the spectrum when the sun is at zenit, but this is quite far from the typical irradiation. Instead, AM1.5 is almost always used for performance benchmarking of terrestrial PV systems. This is the spectrum when the sun is positioned 48 degrees below zenit. The intensity of the sunlight is usually measured in suns, where 1 sun is 1000 W/m^2 or 100 mW/cm^2.

2.2 The p-n junction

When the photons in the sunlight enter the semiconductor, they can be absorbed by exciting an electron from the valence band to the conduction band. This process creates a so-called electron-hole pair. In a direct-bandgap semiconductor, such as InP, the probability for such a transistion is high and most above-bandgap photons are absorbed within about 1 μm. Silicon, which is the most used material for solar cells, has an indirect bandgap which severely reduces the transition probability. Therefore, Si solar cells are typically a few hundred μm thick in order to have sufficient absorption.

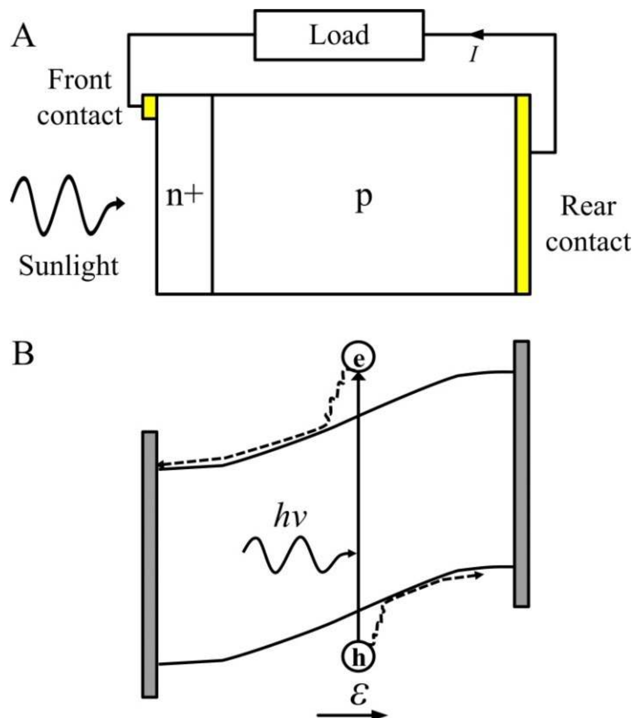

Figure 2.2 *A) Drawing of a p-n junction solar cell, B) Band structure, showing how an electron-hole (e-h) pair is created through the absorption of a photon, hν, and how the carriers are separated by the built-in electric field, ε.*

The excited electrons are not in equilibrium, and will tend to recombine with the holes. Therefore, the holes and electrons must be separated. This can be done in different ways, but high-performance solar cells are based on a semiconductor which has been doped to form a p-n junction. The built-in electric field created by the p-n junction drives the electrons and holes into opposite directions, creating a

net current when they reach the contacts. In practice, most of the device is lightly p-doped to reduce recombination of the comparatively slow holes. At the front is a thin, highly n-doped layer to reduce contact resistance. The extent of the depletion region depends mainly on the p-doping level. It is also possible to use a p-i-n doping profile, with thin, highly p- and n-doped regions, separated by a thick i-region. Such a structure makes it easier to control the length of the depletion region.

2.3 Current-voltage characteristics

The p-n junction must be electrically connected to an external load, as shown in Fig. 2.2A, in order to generate a useful power. The current density, J, through an illuminated p-n junction under bias V is given by [14]:

$$J(V) = -J_{SC} + J_0(e^{qV/kT} - 1) \tag{2.1}$$

Here, J_{sc} is the short-circuit current density, which is the photocurrent generated by the sunlight. J_0 is the saturation current, which is related to the amount of recombination which occurs in the diode, and should be small in a good device. The equation is written using current densities rather than currents, in order to make the parameters comparable between devices of different area. Finally, k is Boltzmann's constant and T is the temperature. Thus, the net current consists of a constant, photogenerated, drift current, J_{sc}, and an opposite diffusion current which increases exponentially with the bias V.

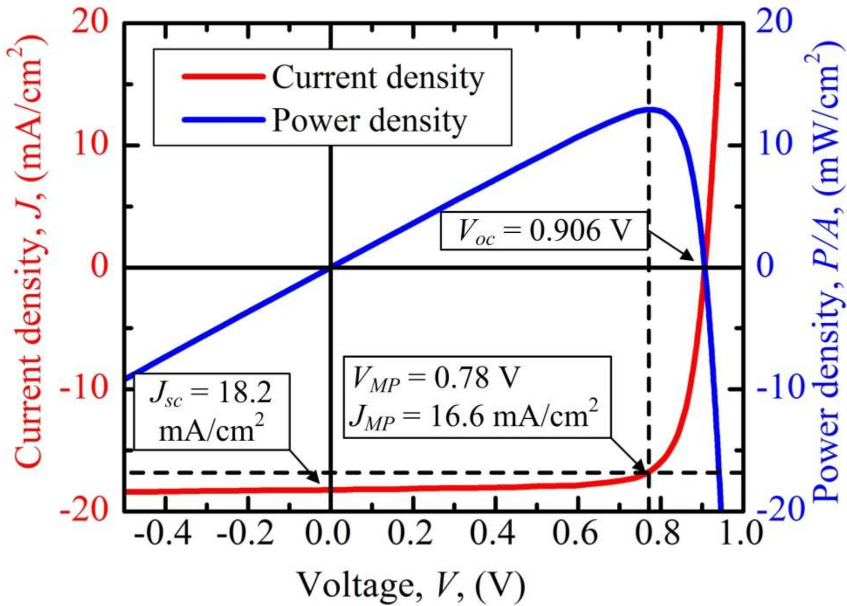

Figure 2.3 *The current density (red) and power density (blue), vs. bias voltage, for a nanowire solar cell under 1 sun illumination. The dashed lines indicate the maximum power point.*

The power density, P/A, generated by a solar cell with area A is given by $P/A = -JV$. The current density (red) and power density (blue) of a solar cell, as functions of the bias, are shown in Fig. 2.3. At zero bias ($V = 0$), that is, when the solar cell is short-circuited, practically all of the generated electron-hole pairs generate a net current ($J = J_{sc}$). However, since the bias is zero, the power is also zero. When the bias is increased, the power increases as well. At high enough biases the exponentially increasing diffusion current becomes significant and at the open-circuit voltage, V_{oc}, the two current components are exactly equal ($J = 0$). This is the maximum voltage produced by the solar cell, but since the net current is zero the power is also zero.

The so-called maximum power point can be found by calculating P/A as a function of bias V. As shown in Fig. 3.3, this function shows a single maximum, where the voltage, V_{MP}, and current density, J_{MP}, at maximum power, are defined. If the power density is measured in mW/cm^2, the power conversion efficiency (PCE or η) in % is equal to the numeric value of the maximum power density (since 1 sun is 100 mW/cm^2). In the solar cell in Fig. 2.3, the maximum power density is 12.9 mW/cm^2, hence η = 12.9%.

2.4 Efficiency limitations

To maximize the efficiency of the solar cell, the first parameter to consider is the bandgap of the semiconductor. Photons which have less energy than the bandgap will not be absorbed and are wasted. On the other hand, photons with energy larger than the bandgap will create electron-hole pairs with excess kinetic energy, but this excess energy is very quickly lost to heat as the carriers thermalize to the band edges. Only the energy equal to the bandgap can be converted into a useful power. A solar cell with a small bandgap will absorb almost all the sunlight but generate a small voltage, while a large bandgap will give a large voltage but almost zero current. In both cases the output power is close to zero.

Carrier recombination processes must be also considered. A high probability for absorption, which is typical for direct-bandgap III-V cells, automatically also gives a high probability for radiative recombination. The radiative recombination sets a lower limit for the recombination rate in the solar cell. Shockley and Queisser calculated the so-called detailed balance limit, for an ideal solar cell with only radiative recombination. They showed that there is an optimal bandgap which is about 1.1 eV [15], near the bandgap of Si. Slightly more sophisticated models, using the AM1.5 spectrum, give a maximum theoretical limit of about 31% efficiency at 1 sun, with a relatively broad peak in the range 1.0 to 1.5 eV [14, 16]. This limit is commonly referred to as the Shockley-Queisser limit.

So far, only fundamental limitations have been discussed. In real solar cells, there are other loss mechanisms which reduce the overall efficiency below the Shockley-Queisser limit. First, the light needs to be coupled in from the air into the semiconductor, which has a higher refractive index. An untreated semiconductor can reflect as much as 30% of the sunlight, but employing surface structuring and anti-reflection coatings this can be reduced to a few percent [14]. NW arrays are highly textured and have inherent anti-reflection properties [17].

Second, there are non-radiative minority carrier recombination processes from impurities, surface states and diffusion. These can be minimized by using high-purity crystals and surface passivation. The thicker the solar cell, the higher the risk for recombination since the carriers will have to travel further to the contacts. Indirect-bandgap Si solar cells typically show signficantly lower efficiency than direct-bandgap III-V solar cells, since they need to be about 100 times thicker to absorb the sunlight.

In the Shockley-Queisser limit, without non-radiative recombination, indirect Si cells could be as efficient as III-V cells. Experimentally, the record single-junction efficiency is 28.8% for a recent GaAs solar cell [6], while the record for a Si cell is 25% [6]. Such high-performance Si cells require ultra-pure material, however, and

this increases the cost substantially. The average module efficiency in production is therefore only 15% [4].

One way of exceeding the Shockley-Queisser limit is to use concentrated sunlight. In concentrated PV, the sunlight is focused with large-area mirrors or lenses onto small solar cells. Setting $J(V_{oc}) = 0$ in eq. 2.1, and since $\exp(qV_{oc} / kT) \gg 1$:

$$V_{OC} = \frac{kT}{q} \ln\left(\frac{J_{SC}}{J_0}\right) \qquad (2.2)$$

The short-circuit photocurrent, J_{sc}, is proportional to the intensity of the sunlight. If the sunlight is focused X times, V_{oc} will increase by $(kT/q)\ln(X)$. In practice, a common value of X is about 500, which then would increase V_{oc} by about 160 mV. Since $\eta \sim V_{oc}$, the efficiency increases as well. The theoretical limit using concentrated light is about 37% for a single-junction cell [16].

2.5 Multijunction solar cells

The tradeoff between current and voltage in single-bandgap devices, described above, limits the maximum theoretical efficiency to about 31% at 1 sun [14]. A way of circumventing this problem is to stack several p-n junctions with different bandgaps, ordered from high to low bandgap towards the sun (Fig. 2.4). The high-bandgap junction absorbs the high-energy part of the sunlight, and utilizes more of the energy in these photons. At the bottom, a low-bandgap junction can absorb the otherwise discarded low-energy photons.

With multiple band gaps, the maximum theoretical efficiency under concentration increases from 37% to 50%, 56% and 72%, for 2, 3 and 36 junctions, respectively [16]. Obviously, the incremental advantage of adding another junction decreases with the number of junctions. At the same time, the practical complexity increases, which explains why current experimental records have been achieved with 3 junctions.

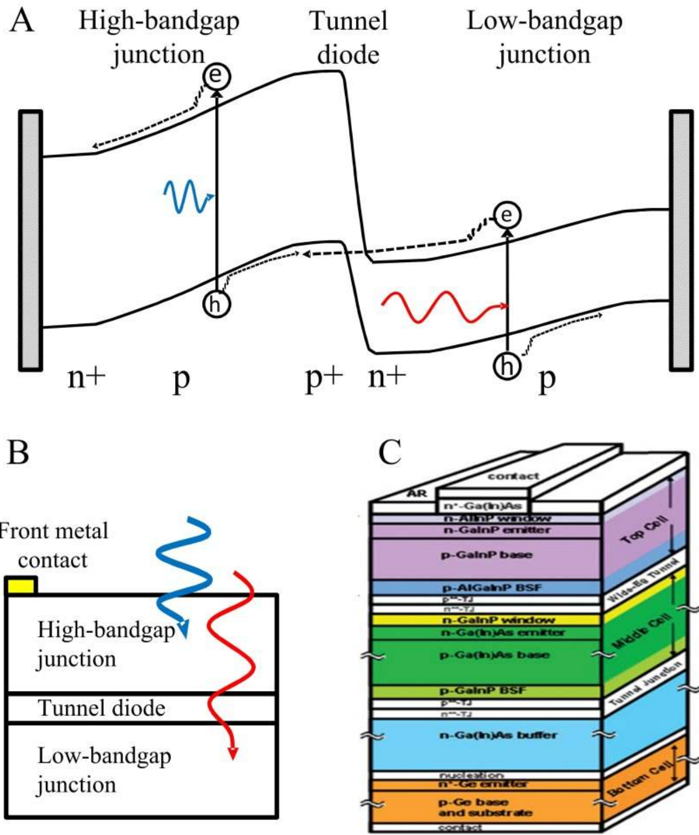

Figure 2.4 Multi-junction solar cells. *A) Band structure, and B) Schematic, of a dual junction solar cell. C) Schematic of a real triple junction solar cell [18].*

If the p-n junctions in a multijunction solar cell were simply connected in series, reverse n-p junctions would form at the boundaries which would block the photocurrent. In principle it is possible to make separate metal connections to the p- and n-side of each junction, but this is unpractical. Instead, modern multijunction cells use so-called Esaki tunnel diodes as connectors.

When a p-n junction has degenerate doping on each side, and the junction is abrupt, the depletion region will be only a few nm long. The thin barrier allows electrons to quantum mechanically tunnel between the n-side conduction band and the p-side valence band. This effect was first discovered in germanium by Leo Esaki [19], who was awarded with the Nobel prize in 1973. By making tunnel diodes in the boundaries between the junctions, photogenerated electrons from the low-band gap junction can tunnel through the depletion region into the valence band of the higher-band gap diode.

Under normal operation, the solar cell is forward biased to the point of maximum power. The carriers which are photo-generated in the bottom cell tunnel from the low-bandgap conduction band to the high-bandgap valence band. The voltages across the tunnel diodes reduce the overall voltage of the solar cell, so to get the maximum power the tunneling must therefore be as efficient as possible.

The tunnel diodes also absorb photons which generate carriers, but the generated current has the wrong direction. Therefore, the tunnel diode is made as thin as possible, and preferably with a bandgap higher than the lower-band gap junction.

The interband tunneling current density, J, is approximately proportional to an exponential factor [20]:

$$J \sim \exp(-4\sqrt{2m^*}E_g^{3/2}/3q\hbar\mathcal{E}) \qquad (2.3)$$

Here, m^* is the reduced effective mass, E_g the bandgap, q the elementary charge, $\hbar$ the reduced Planck's constant, and ε the electric field. To have a high electric field, the junction must be as abrupt as possible which is a challenge during crystal growth. The tunneling is also more efficient with lower effective mass and small bandgap. Because the effective mass tends to increase with the band gap, it is more difficult to make high-band gap tunnel diodes. Since a tunnel diode requires degenerate p- and n-doping, as well as a sharp transition, it is a good test structure both for doping levels and doping gradients.

In a NW-based multijunction solar cell, the requirements on tunnel diodes are more demanding than in a planar device. For instance, if the cross-sectional area of the NWs is 10% of the cell area, the current density will be 1/0.1 = 10 times higher than in an equivalent thin film cell. This means that the voltage drop will be 10 times higher for a given tunnel diode resistance. In paper I, single NW tunnel diodes are demonstrated. While the interband tunneling shows large variation between NWs, the best diodes have sufficient performance for use in multijunction solar cells.

2.6 Nanowire solar cells

The highest-efficiency solar cells are based on III-V materials, but for commercial viability the production costs must be considered as well. Photosynthesis has a very low efficiency, but it still widely used by humans in agriculture partially due to its low cost. Silicon is one of earth's most abundant elements, and thanks to the microelectronics industry there is an enormous knowledge base around Si device processing. The group III materials Ga and In, on the other hand, are relatively rare, and the production volumes are smaller. Therefore, III-V cells are mainly used in space applications while Si-based PV had a 85% market share in 2011 [4].

Crystalline multijunction cells are also limited by lattice matching restrictions. Just like there is an optimum single band gap, there are optimum band gap combinations for dual and triple junction cells. However, in order to grow high-quality thin films, the layers should have similar lattice constants. The lattice-matching requirements limits the available materials, and in practice sub-optimal band gap combinations are used. Lattice matching constraints also affect the available substrates. Due to small Si lattice constant, it is difficult to grow high-quality III-Vs films on Si substrates [21]. Instead more expensive Ge and GaAs substrates are used.

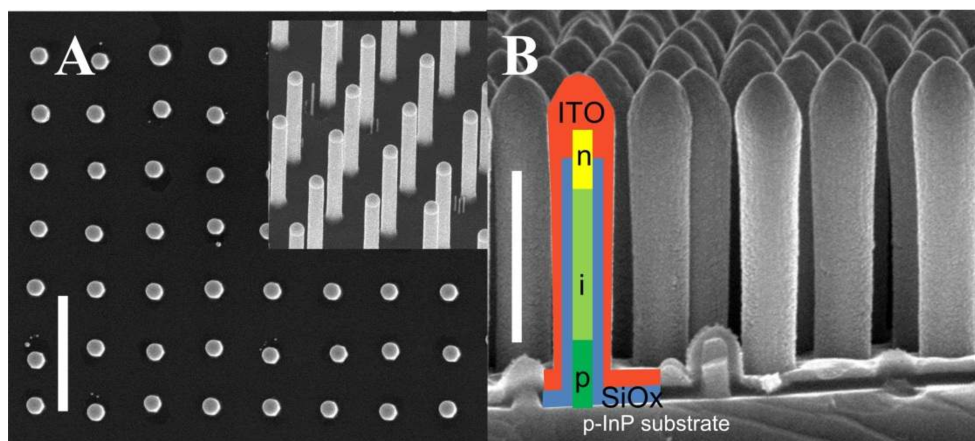

Figure 2.5 *A) Scanning electron microscopy (SEM) images of as-grown InP nanowires, from top. Inset shows the same sample at 30 degrees tilt. B) SEM of finished solar cell. The fabrication process is described in chapter 3.5. Scale bars are 1 μm.*

NWs could overcome some of these limitations. A few years ago it was demonstrated that III-V NWs can be grown epitaxially on Si substrates [7], and more recently graphene [22], which could allow much lower production costs than

thin film III-V cells. It is also possible to grow heterostructures in the NWs with very high lattice mismatch [23], which could allow for optimal matching of the junction bandgaps to the solar spectrum. Surprisingly, even NWs as thin as 200 nm can be efficient absorbers [24]. For these reasons, many research groups are now working on NW-based solar cells using various designs and materials [9-12, 25-34].

Since solar cells rely on p-n junctions, controlled doping is critical for good device performance. In the solar cells which were developed during this thesis, the p-n junctions are defined axially, in the NW growth direction. However, there are also many researchers working on core-shell NW solar cells, where the p-n junction is defined radially [10, 35, 36].

In paper X, InP NW-based solar cells with 13.8% efficiency are demonstrated. Although the NWs only cover 12% of the surface, the photocurrents are almost on par with the best planar InP solar cells. This shows that the NWs have excellent absorption, despite only 180 nm diameter. The efficiency is superior to many other types of next-generation PV technologies with longer development history, such as dye-sensitized [37], quantum dot [38], and organic [6] PV.

3 Nanowire growth

In this chapter, an introduction to NW growth is given.

3.1 Crystal growth

High performance solar cells are based on crystalline semiconductors, which can be fabricated in different ways. To start with, bulk crystal ingots are grown from small seeds. These ingots are then cut into wafers which are polished. For Si-based solar cells, *ex situ* diffusion doping is used to create the p-n junction. In III-V devices, the active layers of the device are normally grown using a vapor phase technique, and the p-n junctions are created with *in situ* doping.

Fundamentally, crystal growth relies on a phase transition from the supply phase to the solid phase. The supply phase can be a liquid, as for bulk ingot growth and in liquid phase epitaxy (LPE), or a vapor, as in metalorganic vapor phase epitaxy (MOVPE). All the NWs in this thesis were grown by MOVPE. The basic idea of epitaxy is to take atoms from the supply phase and move them to the crystal phase, in a way that extends the crystal into the new layers. For the remainder of this thesis, it is assumed that the supply phase is a vapor.

In thermodynamic equilibrium, the system has its lowest energy state. Among other things, this means that moving atoms from one state to the other will increase the total energy of the system. The chemical potential, μ, is equal for the solid and the vapor phase.

Clearly, epitaxy is a non-equilibrium process. To start crystal growth, the chemical potential of the vapor phase is increased by for instance supplying material. This creates a supersaturation, that is, a difference in chemical potential, $\Delta\mu_{v\text{-}s}$, between the vapor and the solid. The system can then reduce its total energy by moving atoms from the vapor to the solid phase.

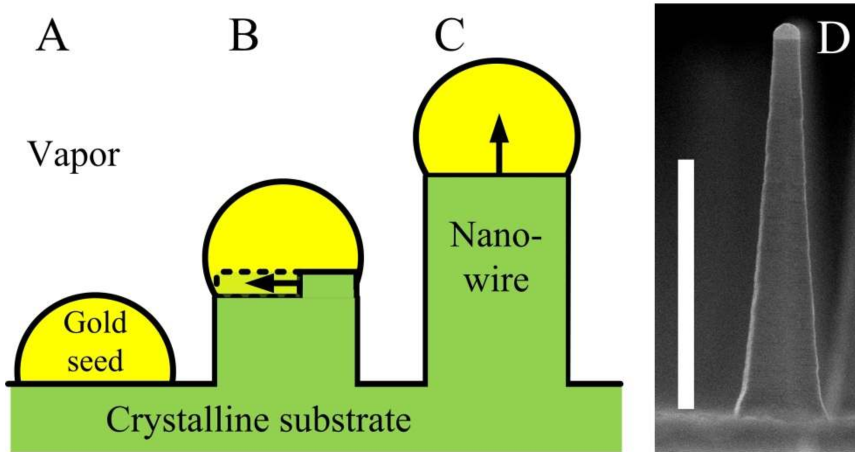

Figure 3.1 Nanowire growth. *A) Gold seed particles on crystalline semiconductor substrate. B) Crystal growth at the interface between the seed particle and the crystal. C) The seed particle is lifted up as the nanowire grows. D) SEM of InP nanowire. Scale bar 1 µm.*

Experimentally, it was found almost 50 years ago by Wagner and Ellis that Si NWs can be grown when Au particles are present on the surface during epitaxy [39]. The crystallisation occurs preferentially at the interface between the gold particle and the crystal (Fig 3.1). As the crystal grows, the seed particle is lifted up. Later, NWs have been observed in many materials, not only semiconductors, and in many types of growth systems. Often, seed particles are used to induce NW growth. Although there are other NW growth mechanisms, it is hereafter assumed that the NWs grow from a liquid metal seed particle. The growth rate for the NWs in this thesis is on the order of 10 µm per hour, which is similar to that of a small child but 3-4 orders of magnitude slower than bamboo plants. Recently, NW growth rates of about 1 µm per second has been demonstrated using so-called aerotaxy [40].

3.2 Nucleation theory

Introducing a seed particle, sometimes termed collector [41], two new relative supersaturations can be introduced: between the vapor and the collector, $\Delta\mu_{v\text{-}c}$, and between the collector and the solid, $\Delta\mu_{c\text{-}s}$. At steady state, $\Delta\mu_{v\text{-}s} = \Delta\mu_{v\text{-}c} + \Delta\mu_{c\text{-}s}$. Since $\Delta\mu_{v\text{-}c}$ must be positive, otherwise evaporation from the seed particle would be seen, it follows that $\Delta\mu_{c\text{-}s} < \Delta\mu_{v\text{-}s}$. That is, the supersaturation between the collector and the solid should not be larger than the supersaturation between the

vapor and the solid. Hence, there must be other reasons why the crystal grows faster at the collector-solid interface [41].

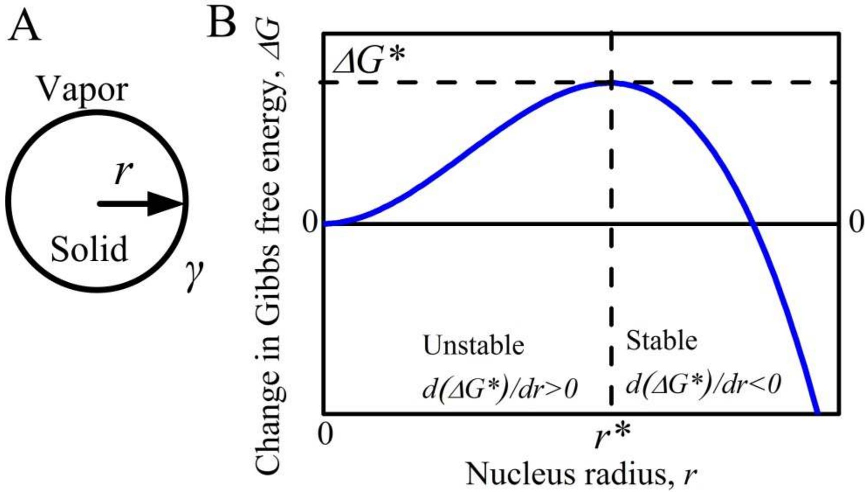

Figure 3.2 *A) Geometry of a spherical nucleus with radius r, B) Change in Gibbs free energy, ΔG, vs. r. The critical radius, r*, and the nucleation barrier, ΔG*, are indicated.*

Instead, classical nucleation theory can be employed [41, 42]. Ignoring NW growth for a moment, this theory assumes that a small crystal nucleus spontaneously forms. Assume first that the nucleus is spherical with radius r, that the molar volume is V_{mc}, and let the supersaturation between the two phases be $\Delta\mu$. Then the Gibbs free energy reduction from the formation of this nucleus is $(4\pi/3)r^3\Delta\mu/V_{mc}$. However, the nucleus also creates a new interface with interfacial energy γ, which increases the Gibbs free energy by $4\pi r^2\gamma$. The total change in Gibbs free energy is then:

$$\Delta G(r) = -\frac{4\pi}{3}r^3\frac{\Delta\mu}{V_{mc}} + 4\pi r^2\gamma \qquad (3.1)$$

In Fig. 3.2, ΔG has been plotted as a function of r. For small nuclei the surface energy term will dominate, while for sufficiently large nuclei the first term will dominate. There is a critical radius, r^*, for which the Gibbs free energy has a maximum, $d(\Delta G)/dr = 0$. Beyond this radius, the nucleus can lower the Gibbs free energy by increasing r (that is, by growing), which means that the nucleus will be stable. For a nucleus with $r < r^*$, the nucleus can reduce the Gibbs free energy by reducing its size, and the nucleus is unstable. The Gibbs free energy at the critical radius is called the nucleation barrier, ΔG^*.

If the supersaturation increases, the first term increases, which reduces the critical radius and the nucleation barrier. This increases the rate of formation of stable nuclei. Since the supersaturation cannot be higher at the seed particle interface, as discussed above, this does not explain why NWs grow.

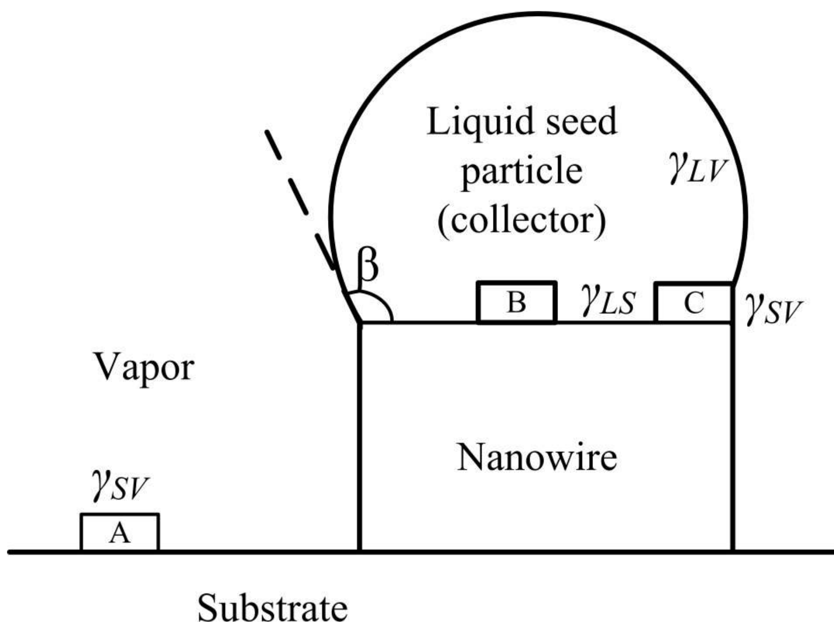

Figure 3.3 Geometry of nuclei at different positions relevant for nanowire growth. *A) Substrate, B) Interface between the seed particle and the nanowire, C) The triple-phase boundary, where the edge of the seed particle meets the edge of the nanowire.*

Instead, the assumption of an isolated spherical nucleus must be dropped. Consider three different nuclei in the NW geometry (Fig. 3.3), in line with models from Wacaser et al. [41] and Glas et al. [43]:

A: Nucleation on substrate or NW side facet.

B: Nucleation at the interface between the NW and seed particle.

C: Nucleation at the triple-phase boundary (TPB).

The top facets of all three nuclei are the same as the pre-existing bottom facets (ignoring heteroepitaxy and crystal faults), so only the side facets will increase the Gibbs free energy.

Assuming a height h and a perimeter length P, the increases in Gibbs free energy, due to the newly created interfaces, are:

$$\Delta G_A = Ph\gamma_{SV} \quad (3.2A)$$

$$\Delta G_B = Ph\gamma_{LS} \quad (3.2B)$$

$$\Delta G_C = Ph\gamma_{LS}(1-x) + Phx\gamma_{SV} - Phx\gamma_{LV}\sin\beta \quad (3.2C)$$

Here, the interfacial energies are the solid-vapor, γ_{SV}, liquid-solid, γ_{LS}, and liquid-vapor, γ_{LV}. In 3.2C, x is the fraction of the nucleus which is in contact with the vapor, and β is the contact angle. The third term in the equation for ΔG_C appears because part of the liquid-vapor interface of the seed particle is removed by the nucleus.

Before continuing, the stability of the liquid seed particle should also be considered. Young's equation at the interface gives the following relation for the horizontal components [44-46]:

$$\gamma_{LS} = -\gamma_{LV}\cos\beta \quad (3.3)$$

It is assumed that the diameter and the contact angles are constant, which is necessary for steady state growth. Note that this contact angle is larger than the contact angle on a flat substrate, for the same material combination, since the solid-vapor interfacial energy of the substrate must be considered in that geometry. The equation shows that β must be larger than 90 degrees to maintain a stable interface, and after growth contact angles of 100-120 degrees are typically observed. That is, γ_{LS} should be smaller than γ_{LV} for realistic contact angles.

For semiconductors, γ_{SV} is typically 1-3 J/m^2 [47]. For gold (Au), which is by far the most used seed material, γ_{LV} = 1.15 J/m^2 [48]. For III-V materials, the group III elements (Al, Ga, In) are metals with high solubility in Au, while the regular group V elements (As, P, but not Sb) show low solubility in Au. Therefore, it is reasonable to assume that the seed particle is a binary liquid metal, consisting of Au and the relevant group III material, for which γ_{LV} is generally unknown. The group III metals (Al, Ga, In) all have lower surface energies, 1.05, 0.72, and 0.56 J/m^2, respectively. In addition, the low-energy component of a binary metal typically tends to segregate to the surface to minimize the energy [49]. It can therefore be assumed that $\gamma_{LV} < \gamma_{SV}$. To summarize, it can be assumed that the following relation holds in most cases: $\gamma_{LS} < \gamma_{LV} < \gamma_{SV}$.

Now the three nuclei in Fig. 3.3 can be compared, starting with the A and B nuclei. Assume first that the seed particle is in equilibrium with the vapor, so that the supersaturation relative to the solid will be the same for both nuclei ($\Delta\mu_{c\text{-}s} \approx \Delta\mu_{v\text{-}s}$). Since $\Delta G_A > \Delta G_B$, the critical radius and the nucleation barrier will be lower at B. This will lead to faster growth at the seed particle-NW interface, B, than at the substrate – vapor interface, A. More realistically, the supersaturation will be lower in the seed particle, which reduces the difference between A and B. However, the lower surface energy of the B nucleus is one possible, and quite general, mechanism, with which the experimentally observed NW growth [41, 43, 50] can be explained. Other possible mechanisms, such as catalytic reactions on the surface of the seed particle [51], could of course be considered as well.

The C nucleus is a bit more complicated, but it can be shown that for realistic values of contact angles and interfacial energies, $\Delta G_C < \Delta G_B$ [43, 44]. In this case, it can be safely assumed that the supersaturation at C will be at least as high as at B, since C is in direct contact with the vapor. Thus, the nuclei will tend to form at the TPB (at C) under most conditions, which is important for the discussion of polytypism as discussed in section 3.4.

Once a stable nucleus has formed, independent of the position of the nucleus, new sites for growth are created at the sides of the nucleus. Since growth at these sites does not create any new interfaces, the nucleation barrier is zero. The lack of nucleation barrier leads to so called step flow growth, which is fast (see Fig. 3.1C).

During step flow growth, substantial amounts of material is consumed which lowers the supersaturation. This increases the nucleation barrier, making it unlikely that another layer is immediately nucleated. Instead, the supersaturation increases with mass transport, as discussed below, until the nucleation barrier is sufficiently reduced. This process has been observed *in situ* in transmission electron microscopy (TEM) [52].

3.3 Mass transport

The material for NW growth has to be supplied to the seed particle. The more efficient this supply process is, the quicker the supersaturation increases after step flow growth, and the quicker the NW will grow. In Fig. 3.4, a few keys steps in mass transport are shown together with some parasitic processes. It is assumed that the NWs are grown from Au seed particles in MOVPE.

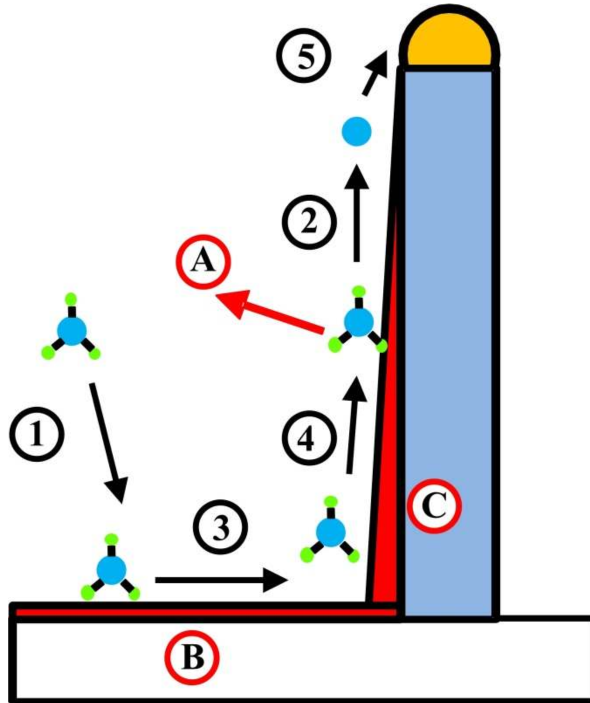

Figure 3.4 Mass transport in nanowire growth. *The various steps, which are explained in the text, are numbered from 1 to 5. The parasitic processes, in red, are labeled A, B and C.*

3.3.1 Transport in carrier gas.

The flow of gases precursors is controlled by the MOVPE system using mass flow controllers. The gas in the reactor is a dilute solution of precursors in a large flow of carrier gas (usually H_2). The gases are supplied at room temperature, while the sample is heated to between typically 400 ºC and 1000 ºC. Since the crystal growth at the sample consumes growth material, and since the gas expands due to the high temperature, there is a concentration gradient between the main part of

the carrier gas and the sample. This gradient make the precursors diffuse, in the gas phase, to the sample surface.

3.3.2 Pyrolysis

In MOVPE, the group III and V constituents are not supplied as elements but in the form of small precursor molecules. For instance, InP growth is usually done with phosphine (PH_3) and the metalorganic molecule trimethyl indium (TMIn). The metalorganic precursors have given MOVPE its name. At room temperature, these molecules are stable, which allows for convenient handling.

The growth elements (e.g. In and P) must be made available through pyrolysis, or decomposition, of the precursors, before these can enter the seed particle. The pyrolysis in MOVPE is an important and complex process, especially at the relatively low temperatures at which NWs are grown. The pyrolysis increases with temperature, up to a point at which practically all molecules decompose and the pyrolysis is said to be complete. This temperature is usually higher for the group V hydrides than for the group III metalorganics.

One distinguishes between homogenous pyrolysis, in the gas phase, and heterogeneous pyrolysis, which occurs at a surface. It is usually found in MOVPE that the heterogenous pyrolysis is significantly more efficient than the homogenous one. For instance, the pyrolysis of PH_3 occurs at about 350 °C lower temperatures in the presence of an InP surface [53].

The pyrolysis is often also more efficient in the presence of other molecules. The pyrolysis temperature of PH_3 can be reduced by 100 °C in the presence of TMIn [53]. This is not so surprising, since the pyrolysis of TMI generates methyl groups (CH_3) which lack one hydrogen atom to form stable methane molecules (CH_4). These hydrogen atoms can be supplied from the PH_3 molecules, leaving atomic P.

The interaction between precursors and the substrate makes MOVPE a complex process. From a technical perspective the slow homogenous pyrolysis is advantageous, however, since an efficient homogenous pyrolysis would allow parasitic formation of non-epitaxial III-V nuclei in the gas phase.

3.3.3 Surface diffusion on substrate

The precursor molecules land on the substrate and become loosely bound (physisorbed). Since they are loosely bound they can diffuse quite efficiently on the substrate surface.

After pyrolysis, as described above, the atoms (for instance In) may continue to surface diffuse. The diffusion rate varies between different molecules and different

elements. A general trend is that the group III precursors and atoms have much longer diffusion lengths than their group V counterparts. Surface diffusion is a thermally activated process.

3.3.4 Surface diffusion on NW side facets

The precursors also diffuse on the NW side facets. This process is similar to the substrate diffusion, but the NW side facets can have other orientations or even crystal structures which can affect the diffusion rate.

3.3.5 Incorporation in seed particle

Once the precursors reach the liquid seed particle, the sticking coefficient is high and the diffusion stops. The group III elements, which are metals, can be accommodated in high concentrations in the seed particle, but the group V elements have quite low solubility.

3.3.6 Parasitic processes

Far from all material supplied into the MOVPE reactor is incorporated into the NWs. These are a few key parasitic processes which can reduce the NW growth rate (Fig. 3.4):

A. Desorption. The growth precursors can desorb from the substrate.
B. Substrate growth. Although the nucleation barrier is higher at the substrate, some growth will occur.
C. Radial NW growth. This process is similar to substrate growth, but can have a different rate since the surface facets (and therefore surface energies) are different.

Radial NW growth is commonly referred to as "tapering", since the NWs often get a conical shape as the time for radial growth is longer at the base. Aside from being a parasitic process which can reduce NW growth rate, it can also affect the performance of axially defined NW devices.

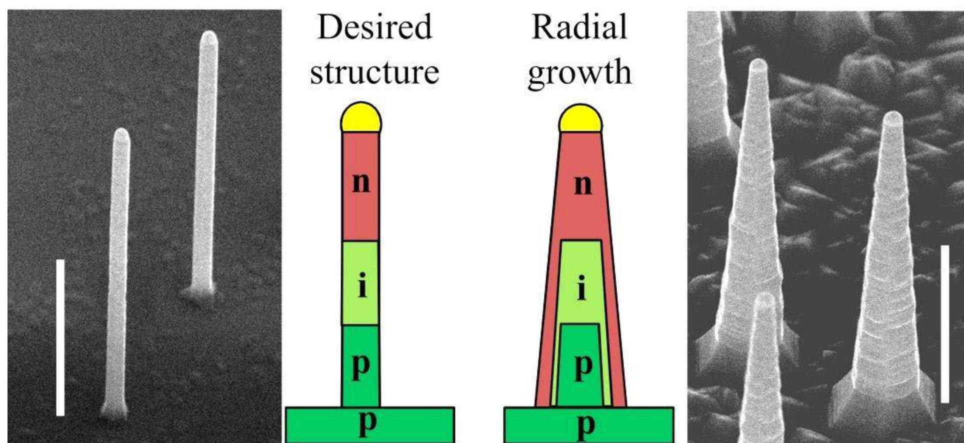

Figure 3.5 Radial growth (tapering). *Desired p-i-n doped nanowire for solar cells (left), and structure resulting from radial growth (right). The main current paths are indicated with arrows. The SEMs show InP nanowires grown with (left) and without (right) HCl, scale bar 1 µm.*

For example, in a p-i-n doped structure for solar cells, as shown in Fig 3.5, the desired structure will have a well-defined depletion region in the vertical growth direction. If there is radial growth as well, p-n junctions will form radially and to the substrate. This can lead to reduced performance.

To reduce the radial growth, the temperature and/or the group V flow are normally reduced relative to planar growth conditions [54]. Another option, which has been used extensively in the experiments for this thesis, is to use *in situ* etching with hydrogen chloride (HCl) [55, 56]. This method can completely prevent radial growth, as shown in Fig. 3.5, which was also confirmed by electrical measurements in paper VIII.

3.4 Polytypism

The regular III-V materials all have the cubic zincblende (ZB) crystal structure in bulk. For NWs, already the early work by Hiruma et al. during the 90´s showed that GaAs and InAs NWs exhibit a mix of zincblende and wurtzite (WZ) crystal structure [57]. Later, Johansson et al. showed that GaP NWs can exhibit ZB segments with rotational twins [58], and NW polytypism has lately become an intense field of research [43, 50, 59]. *In situ* doping strongly affects the polytypism, as will be discussed in section 5.3.

It is experimentally observed that the crystal faults typically occur orthogonal to the growth direction. Each plane forms a perfect crystal layer, and its crystal structure and rotational orientation is determined by the initial nucleus. During the step flow growth, there is a high barrier for changing the crystal structure. As discussed in section 3.2, it is normally advantageous for NWs to nucleate at the TPB. The basic driving force for WZ formation is usually identified as a lower surface energy at the solid-vapor interface γ_{SV}. Thus, nucleation at the TPB is a necessary requirement for the formation of WZ [60].

The polytypism can have strong effects on the optical and electrical properties of the NWs. Normally, WZ has a slightly larger bandgap than ZB for the same material (1.49 eV vs. 1.42 eV for InP [61]), and in addition there is often a type II band offset [62]. For a NW with a mixed crystal structure, the electrons will then collect in the ZB segments while the holes collect in the WZ segments. The crystal structure affects the optical spectra and the lifetimes as observed in photoluminescence (PL) [63, 64]. The electron transport along the NW axis is perpendicular to these crystal faults. In paper VIII it is shown that the ZB segments in polytypic InP NWs trap electrons and reduce the carrier concentration as well as the mobility. Similar observations have previously been done in InAs NWs [65, 66].

3.5 Fabrication of nanowire solar cells

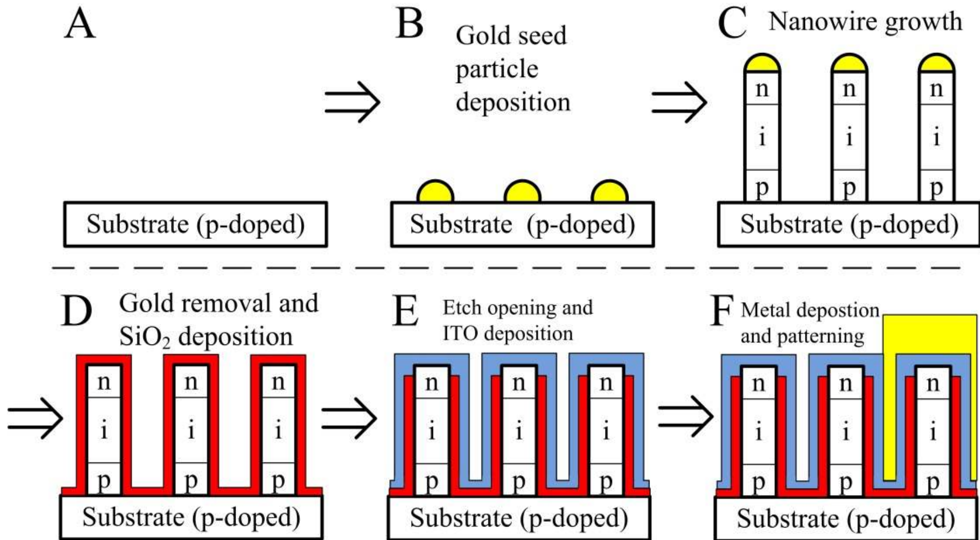

Figure 3.6 Fabrication of nanowire solar cells. *The red, blue and yellow colors indicate SiO_2, ITO and metal, respectively. The steps are explained in the main text. An SEM of processed nanowires can be found in Fig. 2.5.*

The NW growth is only one step out of many in the fabrication of NW solar cells (Fig. 3.6):

A: First, a crystalline substrate is chosen. This can be Si, or as in this thesis, InP. The doping of the substrate is chosen after the overall polarity of the solar cell, which in this case is n-type on top and p-type at the bottom.

B: Gold seed particles are deposited, using nanoimprint lithography [67], electron beam lithography (EBL), or aerosol deposition [68, 69].

C: NW growth.

D: Gold removal with wet etching [70], followed by growth of an insulating SiO_2 layer (shown in red) by atomic layer deposition (ALD).

E: Coating with polymer, which is thinned down to expose the NW tips. Wet etching of SiO_2 to expose the n-type top segment. Sputter deposition of indium tin oxide (ITO, shown in blue) as a transparent top contact.

F: Evaporation of metal (shown in yellow) for front contacts. Patterned with UV lithography.

4 Dopant incorporation

Controlled doping of NWs is necessary to make p-n junctions and tunnel diodes for solar cells. Traditional microelectronics mainly relies on *ex situ* doping with diffusion and ion implantation, but it is difficult to position the dopants vertically in a NW device with these techniques. Since the differently doped layers are defined vertically, in the growth direction, it is natural to incorporate dopants *in situ* crystal growth. *In situ* doping of III-V NWs was demonstrated already two decades ago by the group of Hiruma [71]. Later, Lieber's group doped Si NWs [72].

In situ doping is done by intentionally adding impurities during growth, which replace some of the atoms in the host lattice. For n-type doping the impurity should have one extra valence electron compared with the atom which it replaces, and it is then called a donor. For p-type doping the impurity should instead have one less free electron, and it is then called an acceptor.

For n-type doping of III-Vs it is natural to use elements which have one more valence electron compared with the group V element, that is, to use group VI elements. Sulfur (S) is such an element, which replaces P in the InP lattice and thereby provides one additional free electron. Conversely, it is natural to use group II elements such as zinc (Zn) for p-type doping. Group IV elements, such as Si, are also used for doping since they tend to prefer either a group III or group V position in the lattice.

Just like the main elements, the dopants in MOVPE are supplied as molecules which decompose at the hot substrate. Both metalorganic precursors such as diethyl zinc (DEZn) and hydride precursors such as hydrogen sulphide (H_2S) are used, and for a given dopant there may be several different precursors available. Since the growth temperature for NWs is often 100-300°C below that of the corresponding thin films, the pyrolysis may be important for precursors which are completely cracked in thin film growth. To get the p-i-n doping structure which is desired for InP solar cells, a p-doped segment is first created by growing with a DEZn flow together with TMI and PH_3. For the i-segment, the DEZn is turned off, and finally the top n-segment is grown with H_2S.

To measure the efficiency of the doping, a segregation coefficient, k, can be defined. This is the ratio between the dopant precursor concentration in the vapor phase, c_v, and in the solid crystal, c_s. The segregation coefficient has been

investigated in thin film growth, and depends on dopant, dopant precursor, host material and growth temperature. However, for a given set of precursors and a given growth temperature, there is usually a relatively broad range where the solid concentration is proportional to the vapor concentration, i.e. where k is a constant.

4.1 Axial growth

In order for dopants to be incorporated in the axial NW growth, they must be present at the NW-seed particle interface during step flow growth. Although the NWs are grown from vapor phase precursors, the growth and doping at the interface could be seen as a nanoscale local liquid phase epitaxy (LPE) system [73], where the dopant has a liquid concentration c_L. The solid dopant concentration is given by the segregation coefficient, k_{SL}: $c_S = k_{SL}\ c_L$. The segregation coefficient here may differ from the ones established in regular LPE, due to the presence of the seed metal. The segregation coefficients known from regular LPE show great variation between different dopants for the same semiconductor material, or between different semiconductors for the same dopant. For instance LPE of InP shows dopant segregation coefficients which vary from 30 for Si to $2x10^{-3}$ for Sn [74].

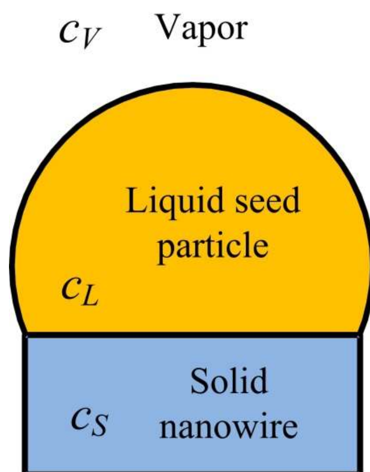

Figure 4.1 Schematic of the dopant concentrations in vapor-liquid-solid NW growth. *The desired result is a certain solid concentration, c_s, but it is the vapor concentration, c_v, which is controlled by the growth system.*

Dopants show great variation in their solubility in liquid metals. Some, like Zn, are themselves metals which form compounds with Au. Others, like S, have low

solubility, which means that even if c_v for S is set high, the c_L will likely be low. If the incorporation is efficient, that is if k_{SL} is high, it may still be possible to reach high doping levels. This is indeed the case for S-doping of InP, which was investigated in paper IV. If the solubility is low and the incorporation is inefficient, it will be difficult to achieve high doping levels. Since the solubility may vary between different seed particle metals, there may also be significant differences between doping of self-seeded (for instance Ga-seeded GaAs) and Au-seeded NWs.

The solubility of the dopants in the seed particle can also be expected to have strong influence on the gradient when the dopant source is turned on or off and the steady state assumption no longer holds. This gradient can be of critical importance for devices such as tunnel diodes. For dopants with low solubility it should in principle be possible to achieve gradients as sharp as those achieved in thin film growth.

A test of the sharpness of doping profiles can be achieved by creating interband (Esaki) tunnel diodes, which require p-n-junctions with a depletion width on the order of 10 nm for successful operation. In paper I, tunnel diodes made from a junction between S-doped InP and Zn-doped GaAs are demonstrated. In this case, the low solubility of S is probably advantageous. However, in paper VII the reverse order of dopants, used in InP NWs, also shows tunnel diode characteristics. Apparently, any memory effect of the Zn dopant does not severely increase the length of the depletion length.

For compound semiconductors such as III-Vs, the relative fluxes or partial pressures of the anions and cations must be considered. It is well-known in thin film growth that e.g. a relatively low AsH_3 flow enhances S incorporation in GaAs [75], since S is incorporated on group V lattice sites. Although the V/III ratio in the vapor may be quite high, the ratio in the seed particle is normally much lower since the group V elements have lower solubility. The low local V/III-ratio suggests that p-type doping of III-V NWs would be relatively more difficult compared with thin films, but as discussed above the solubility of p-type dopants in the seed particle is typically much higher than that of n-dopants. These effects are even more critical when using amphoteric group IV dopants, such as Si, which can induce n- or p-type doping depending on which lattice site they occupy.

4.2 Incorporation in radial growth

Radial growth may be desired in so-called core-shell NW devices, which are being investigated for PV and other devices [10, 76]. However, for axial NW devices, radial growth can lead to short-circuiting and is therefore generally undesired. Several authors have found the dopant incorporation in the radial growth to be more efficient than the axial growth [73, 77].

Doping in the radial growth is inuitively more similar to thin film growth than the axial one, since the elements come directly from the vapor phase, not via the seed particle. Many lessons learned from doping of thin films should also apply to doping of radial NW growth. One difference is the NW side facets. Most of the research on thin films has been done for the commercially dominant (001) substrates. NWs, however, show many different facets, also depending on the crystal structure. The facets strongly affect the shell growth rates [78, 79] (paper III). From thin film experiments it is also known that the substrate orientation and miscut can increase or decrease the dopant incorporation by one order of magnitude [80].

4.3 Carrier generation

So far, the incorporation of dopants rather than the carrier generation has been considered, although it is the carriers rather than the dopants which are technically useful. The dopants are the impurity atoms which should provide the carriers, for instance a Zn dopant atom should provide one extra free hole in InP. However, this is an ideal case, and there are several effects which could reduce the carrier concentration (p or n) below the dopant concentration (N_A or N_D).

First, the dopant must incorporate in the correct position in the lattice. In the case of Zn-doping of InP, the hole concentration saturates above a Zn concentration of about $5x10^{18}$ cm^{-3} because the Zn atoms do not incorporate at the desired In positions [81]. Instead, the Zn forms deep levels.

Furthermore, NWs have a large surface-to-volume ratio which may influence dopant incorporation. Theoretical investigations have predicted that it will be energetically favorable for dopants to segregate to the surface [82, 83], although these calculations were done for few-nm diameter NWs with much higher surface-to-volume ratio than typical NWs. Xie et al. experimentally investigated doped Si and Ge NWs and found a transition diameter of around 22 nm [84]. Below this diameter the doping in the bulk of the NW was low and most of the dopants were found in a surface layer, while for larger NWs there was significant bulk doping together with a highly doped shell.

In paper IV, S-doping of InP NWs was investigated. Using TEM (see section 6.3), we observed S concentrations up to 0.9% in the highest doped NWs. This would correspond to a dopant concentration of 3.6×10^{20} cm^{-3}, but optical measurements indicated much lower electron concentrations. The results suggest that much of the S was incorporated at the surface, which was also supported by TEM line scans across the NW.

Second, the dopants must be ionized, so that the carriers are actually free. For n-type doping of regular III-Vs this is not a problem (at room temperature), since the binding energy (6 meV) is far less than kT (26 meV). Holes have larger binding energies however, around 40 meV in InP, and hundreds of meV in GaN. Theoretical predictions [85] as well as experiments [86] have shown that the ionization energy of dopants increases in thin NWs due to electrostatic effects.

Finally, the carrier concentration may be spatially different from the dopant concentration. While the dopant atoms are part of the lattice, the carriers are free to move. For instance, surface states may locally shift the Fermi level and increase or decrease the carrier concentration.

4.4 Summary

In Fig. 4.2 a list of references to articles concerning *in situ* doping of semiconductor NWs is presented, sorted according to the NW material. A more extensive list is included in paper VI.

Material	**n-type**	**p-type**
GaP	S [87]	NH_3 [88]
GaAs	Si [10, 89, 90], SiH_4 [91], Si_2H_6 [92, 93], GaTe [94, 95], TESn [96]	Si [10, 73, 97], TMGa [92], DEZn [91, 98, 99] (paper I), Be [90, 94, 95],
InP	Si [100], SiH_4 [12], Te [25], TESn [101], H_2S [99, 102] (paper I, IV, VIII), Se [103, 104]	Zn [25, 104], Zn_3P_2 [105], DMZn [101], DEZn [9, 12, 45, 102, 106] (paper II, VII)
InAs	$SiBr_4$ [107], TESn [107], H_2S [107, 108], DTBSe [107], Si_2H_6 [108], DETe [108]	Be [109], CBr_4 [108]

Figure 4.2 Table of references regarding in-situ doping of semiconductor NWs. *This list shows the materials which have been used in this thesis. A more comprehensive list can be found in paper VI.*

Despite all the complex mechanisms discussed here, the overall tendency seems to be that NWs can be doped to similar levels as the corresponding thin films [110]. Although an accurate determination of doping levels is challenging, as will be discussed in chapter 6, indirect evidence of high doping can be found in the performance of devices such as tunnel diodes [99] and tunnel-FETs [111], as well as the nano-sized ohmic contacts formed to many NWs.

5 Effects of *in situ* doping on nanowire growth

In this chapter, different types of effects from *in situ* doping on NW growth are discussed.

5.1 Growth rate

The *in situ* addition of dopant precursors often affects the NW growth rates, both axially and radially. Fig. 5.1 shows an overview of how the dopants which have been investigated in this thesis, affect the axial growth rate of InP NWs.

In paper IV it is shown that H_2S increases the axial growth rate about three times, while the radial growth is strongly reduced. In this case, it is probable that the sulfur passivates the substrate and the NW side facets, which reduces the parasitic growth and increases the growth rate. If the NWs are grown with HCl, which in itself eliminates radial growth, the NW growth does not increase with H_2S (paper VIII).

Dimethyl zinc (DMZn) also strongly increases the growth rate [101], but, as shown in paper II, DEZn does not affect the growth rate much. Clearly, Zn itself is not responsible for the change in growth rate, but rather the precursor molecules. This could be explained by the higher pyrolysis temperature of DMZn, which may allow the precursor to act as a surface passivator of the competitive radial growth.

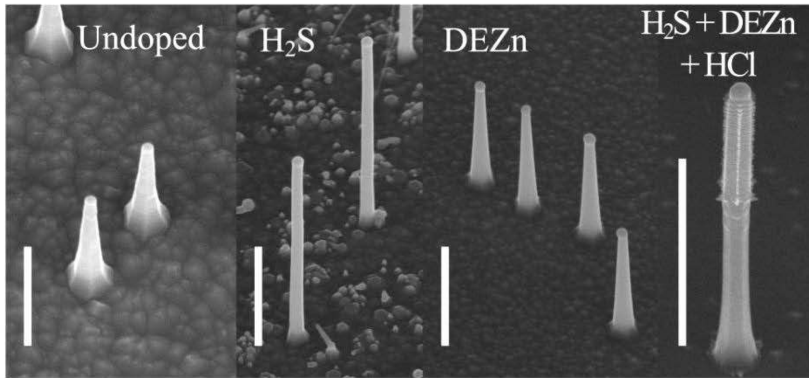

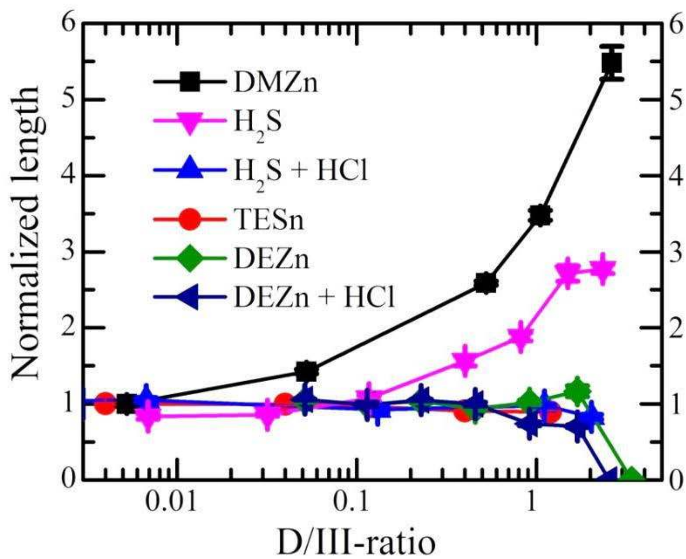

Figure 5.1 Effects of* in situ *doping on nanowire growth rates. *(top) SEM images of InP NWs grown with different doping precursors. The right-most image shows a nanowire which was doped with H_2S at the bottom and DEZn at the top, with HCl supplied throughout the growth. Tilt 30 degrees off normal, scale bar 1 µm. (bottom) Plot of the length of InP NWs vs. dopant to group III molar fraction (D/III-ratio). The lengths were normalized with the length of the undoped reference NWs for each series.*

5.2 Growth instability

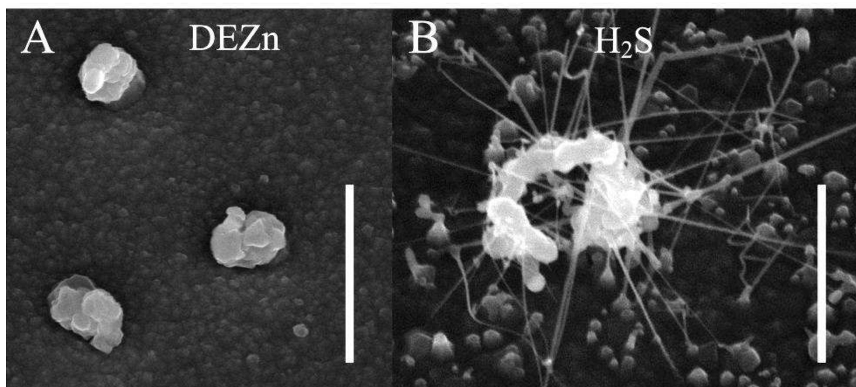

Figure 5.2 Effects of too high dopant molar fractions on InP nanowire growth.
A) DEZn, B) H_2S. Scale bar 1 µm.

At very high molar fractions, most dopants are detrimental to InP NW growth. Sufficiently high DEZn molar fractions completely prevent InP (and GaAs) NW growth, as shown in Fig. 5.2A. This is the case both with (paper VII) and without (paper II) HCl. The seed particles seemingly crawl around on the substrate without any clear growth direction. Since DEZn leads to increased contact angles, it is likely that the seed particle wets the NW side facets at too high molar fractions.

H_2S also destabilizes growth at too high molar fractions (Fig. 5.2B, paper IV), but in a different way from DEZn. Increasing H_2S molar fractions eventually lead to kinked NWs which grow in non-vertical directions, as well as substrate growth and formation of many very thin NWs. When H_2S is combined with HCl the growth is stable also for very high molar fractions, but the doping levels are about one order of magnitude lower (paper VIII).

In none of the cases in this thesis has doping increased the radial growth, but there are such examples in the literature. For instance, Rigutti et al. found that Si-doping of InP NWs increased the tapering and reduced the growth rate [100].

5.3 Structural effects

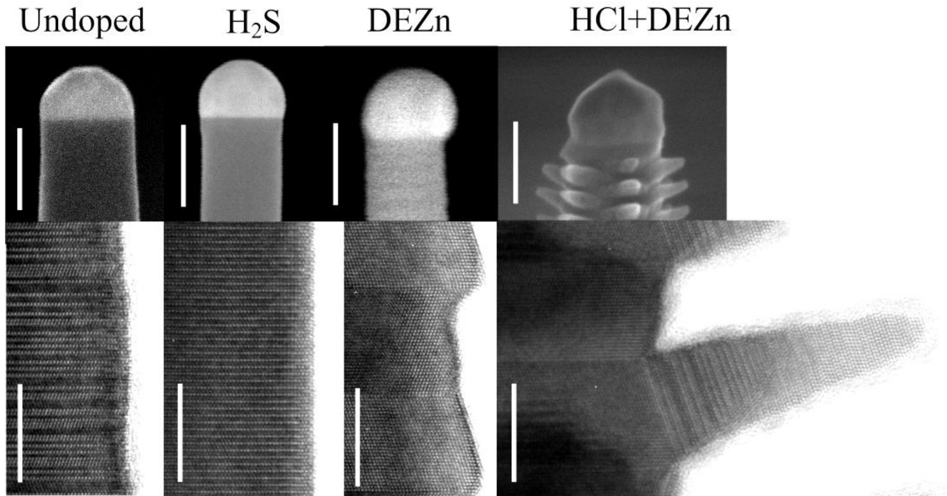

Figure 5.3 Structural effects of* in situ *doping. *SEM (top row, scale bars 100 nm) and TEM (bottom row, scale bars 10 nm) of doped InP NWs. The right-most NWs are from the same sample as the thesis cover. TEM courtesy of Martin Ek.*

As discussed above, III-V NWs typically show a mix of the ZB and WZ crystal structures. This is also seen in Fig. 5.3. As shown in paper VIII for InP NWs, and as previously observed in InAs NWs [65, 66], this polytypism affects both the effective carrier concentration and the mobility. Since the polytypism is sensitive to growth parameters such as V/III-ratio and temperature, it is not surprising that it is also affected by *in situ* doping. Thus, doping affects the crystal structure, and the crystal structure in turn affects the carrier concentrations.

Already in 1973, Givargizov reported periodic instabilities and faceting during growth of undoped Si and Ge NWs [112]. He found that small additions of $AsCl_3$ removed these instabilities, and also observed that this dopant precursor improved the wetting of the seed particle. Much later periodic faceting and periodic twinning was observed in In-doped ZnO NWs [113] (see fig 4C).

Later, Algra et al. reported that undoped InP NWs had grown with a mixed crystal structure, but that additions of DEZn induced growth in pure ZB crystal structure with rotational twins [106]. Higher DEZn flows created a so-called twinning superlattice, where the distance between the twins was highly regular.

In paper II, the InP NW doping with DEZn was investigated and a gradual transition to ZB with twinning was observed [45], similar to the results of Algra et

al. [106] (see also Fig. 5.3). We also reported strong effects on the wetting of the seed particle. In line with the observations by Givargizov we found that the periodic twinning correlated with a poor wetting of the seed particle, that is, a large contact angle, although DEZn had the opposite effect of $AsCl_3$. A transition to ZB with twinning in InP NWs grown with DMZn [101] has previously been shown, which indicates that Zn rather than the precursors are responsible for the crystal structure changes. The effect of DEZn remained when combined with HCl (paper VII, Fig 5.3), although there was also a strong growth on the (111)A facets in this case.

Mirroring the results with the p-dopant Zn, we show in paper IV that the n-dopant H_2S induces growth in perfect WZ crystal structure. When combined with HCl, the tendency to induce WZ is significantly weakened (paper VIII).

5.4 Compositional effects

To this point, doping of single-element and binary materials has been discussed. In these, the basic composition of the host material is fixed. For instance, InP is essentially 50% In and 50% P, even if dopants are introduced. However, with ternary materials the situation is different. For instance $Ga_xIn_{1-x}P$ always has 50% P atoms, but the share of Ga atoms of the total group III atoms (Ga + In), x, depends on the growth conditions [114]. The precursors for Ga (TMGa) and In (TMIn) are different, and they have different pyrolysis behavior and different diffusion lengths. It is therefore not surprising that for a given TMGa/TMIn ratio, different growth temperatures give different compositions [114].

If dopants are introduced, they can also effect the composition in different ways. As discussed above, some dopant precursors, such as sulfur, may act as surface passivators which can affect diffusion lengths. It is also possible that a dopant can have such a high solubility in the seed particle that it affects the equilibrium concentration of the growth elements.

In paper IX, we found that the composition of $Ga_xIn_{1-x}P$ NWs is affected by both DEZn and H_2S, but in different ways. Note that the NWs were successfully p- and n-doped.

5.5 Summary

Dopant precursor	**Growth rate**	**Structural trend**	**Composition in $Ga_xIn_{1-x}P$**	**Reference**
DMZn	Increase	Zinc blende		[101]
DEZn	Weak effect. Prevents growth at high concentrations	Zinc blende		Paper II
DEZn + HCl	Weak effect. Prevents growth at high concentrations	Zinc blende	Decreased Ga	Paper VII, IX
H_2S	Increase	Wurtzite		Paper IV
H_2S + HCl	None	Slightly wurtzite	Decreased Ga	Paper VIII, IX
TESn	None	None		[101]
TESn + HCl	None	Slightly wurtzite		Unpublished
HCl	Complex	Slightly wurtzite		[55]

Figure 5.4 Overview of effects of* in situ *doping on InP and GaxIn1-xP nanowire growth. *The dopant precursors gave the desired p- or n-doping in all of the investigated cases. HCl is used to prevent radial growth [55], not for doping, but it also influences the NW growth.*

In the table in Fig. 5.4, the effects of different dopant molecules on InP and GaInP NW growth have been summarized. *In situ* doping of NWs in many cases shows stronger and more complex effects on crystal growth than for the corresponding planar growth. The effects of doping on e.g. growth rate or crystal structure are also often stronger than the effects of changes in growth parameters such as V/III-ratio. While some of these effects can be problematic, others, such as higher crystal purity or decreased radial growth, can be advantageous for applications.

6 Nanowire doping measurements

The understanding of NW doping is closely related to the ability to measure the doping. Quantitative doping measurements are still a major challenge in NW research, although there has been a strong development in the last years. Electrical measurements have historically been the most important ones, but recently many groups have demonstrated quantitative measurements using other techniques. When discussing doping measurements, it is important to distinguish between techniques that measure the dopant concentration and techniques that measure the carrier concentration.

6.1 Electrical methods

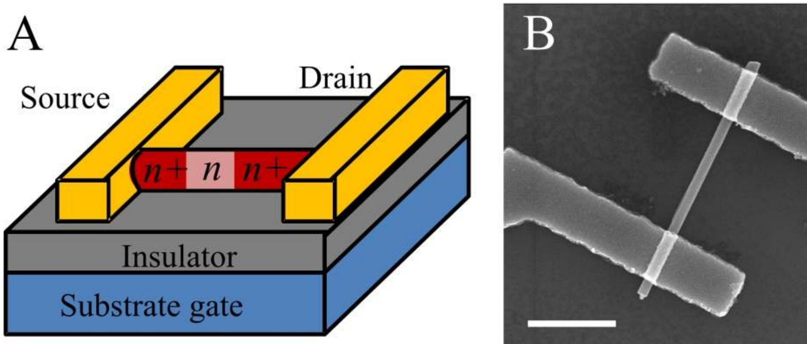

Figure 6.1 NW-FET measurements. *A) Illustration. B) SEM, top-view, of NW-FET. Scale bar 1 µm.*

Traditional Hall measurements are difficult to use due to the small size of NWs, and have only very recently been demonstrated [115, 116]. The first quantitative characterization of doping levels was done by Cui et al. using so-called NW field effect transistors (NW-FET) [72]. This is still the most commonly employed method, also in this thesis. NW-FETs consist of a NW which has been broken off the growth substrate, put on an insulating substrate and contacted on both ends. The conductivity of the NW can be measured by sweeping the source-drain

voltage and measuring the current. The conductivity, σ, is connected to the carrier concentration n as [20]:

$$\sigma = nq\mu \qquad (6.1)$$

where q is the elementary charge and μ is the carrier mobility. By changing the potential of the back gate in the substrate the transconductance can be measured, which can be used to estimate the mobility. In the linear transistor regime, the transconductance is connected to the mobility [20]:

$$g_m = \left.\frac{dI_{SD}}{dV_G}\right|_{V_{SD}=constant} = \frac{C\mu}{L^2} V_{SD} \qquad (6.2)$$

Here, I_{SD} is the source-drain current of the NW-FET, V_{SD} and V_G are the source-drain and gate voltages, respectively, and L is the length of the active region. C is the capacitance, which is usually modelled as a metallic cylinder surrounded by a dielectric some distance from an infinite and flat metallic back gate, leading to the following expression [117]:

$$C = \frac{2\pi L\epsilon_0\epsilon_r}{\cosh^{-1}(\frac{R+h}{R})} \qquad (6.3)$$

where ε_r is the relative dielectric constant, R the NW radius and h the distance between the gate and the bottom edge of the NW. Improved electrostatic control can be achieved by using a top gate [35, 118] or creating a vertical transistor with a wrap gate [119].

In principle, both the carrier concentration and the mobility can be accurately determined with this method. However, many assumptions are made which lead to limitations of the described model, as discussed in detail by Wunnicke [120] and Khanal et al. [121]. First, the dielectric does not surround the NW but is rather a thin film, which leads to a capacitance which is reduced about a factor of two. Second, the model for eq. 3 is based on the assumption of an electrostatically metallic NW, while the NW is in fact semiconducting.

The model also assumes that both the carrier concentration and the mobility are spatially constant. The carrier concentration could be strongly affected by surface states, and for instance InAs NWs have a surface inversion layer which is highly n-type. The mobility could be reduced by scattering near the surface, or increased by a high-bandgap shell [122].

A technical challenge with NW-FETs is making good electrical contacts. This task can be difficult enough with some bulk semiconductors, but NWs pose several additional problems. Before the metal deposition any oxide should be removed, but the small size of the NWs only allows for gentle processing. Additionally,

many contact recipes developed for bulk semiconductors are based on high-temperature annealing, which leads to compounds forming and local drive-in of dopants which have been added to the metal layers. For example, a Pd/Zn/Pd/Au combination has been used for ohmic contacts to bulk p-type InP [123]. At a temperature of around 400 ^{o}C, Pd reacts with InP and the Zn is driven into the InP since the second Pd layer acts as a cap. However, in a nanometer-scale device such as an NW-FET, such reactions may lead to the entire device becoming metallic. The Zn may also diffuse out into the ambient rather than into the NW.

Despite these challenges, ohmic contacts have in many cases been formed to NWs, e.g. p-type [124] and n-type [125] Si, p-type GaAs [98] (paper I) and n-type InP [25] (paper IV, VIII). Of utmost importance is to have a highly doped semiconductor, since it creates a thin Schottky barrier through which carriers may tunnel. With reasonably good ohmic contacts, the contact resistance can be decoupled with transmission line measurements where the channel length is varied. Another technique to separate the contact resistance is using 4-point measurements, but Thelander et al. showed that for InAs NW-FETs with low-resistance contacts the inner probes are invasive [126]. Lower-doped material typically show nonlinear, Schottky-like, behavior [101]. Notably, InAs has a degenerate surface inversion layer which allows ohmic contact formation even to nominally undoped NWs.

Without high-quality contacts to the NW the resistance is normally limited by the contacts rather than the NW channel. Since the back gate affects the contacts and the NW channel simultaneously, poor contacts make the interpretation of both source-drain and gate-sweep measurements difficult. Even without ohmic contacts, the gate-sweep measurements can be used to identify the type of majority carrier in the device (n- or p-type), and an estimate of the carrier concentration can be achieved from the threshold voltage [101].

A strategy to circumvent the challenge with contacts is to highly dope the bottom and top end of the NW, while leaving the middle segment low-doped [127-129] (paper VIII). This type of structure can have very low contact resistance relative to the channel resistance, and allows for devices with doping profiles more similar to planar MOSFETs.

Overall, NW-FET measurements can often give precise data in terms of device resistance and transconductance. Converting these into quantitative material properties such as carrier concentration and mobility is straightforward, but the actual precision is often questionable due to the number of simplifications used.

6.2 Optical methods

Optical measurement methods are attractive because they are often processing-free and therefore potentially simpler and faster than electrical measurements. In photoluminescence (PL), the sample is irradiated with light which creates electron-hole pairs. The electrons and holes recombine while sending out photons, and this luminescence is measured. Typically, the signal in a high purity direct band gap semiconductor is dominated by recombination near the band gap (Fig 6.2A).

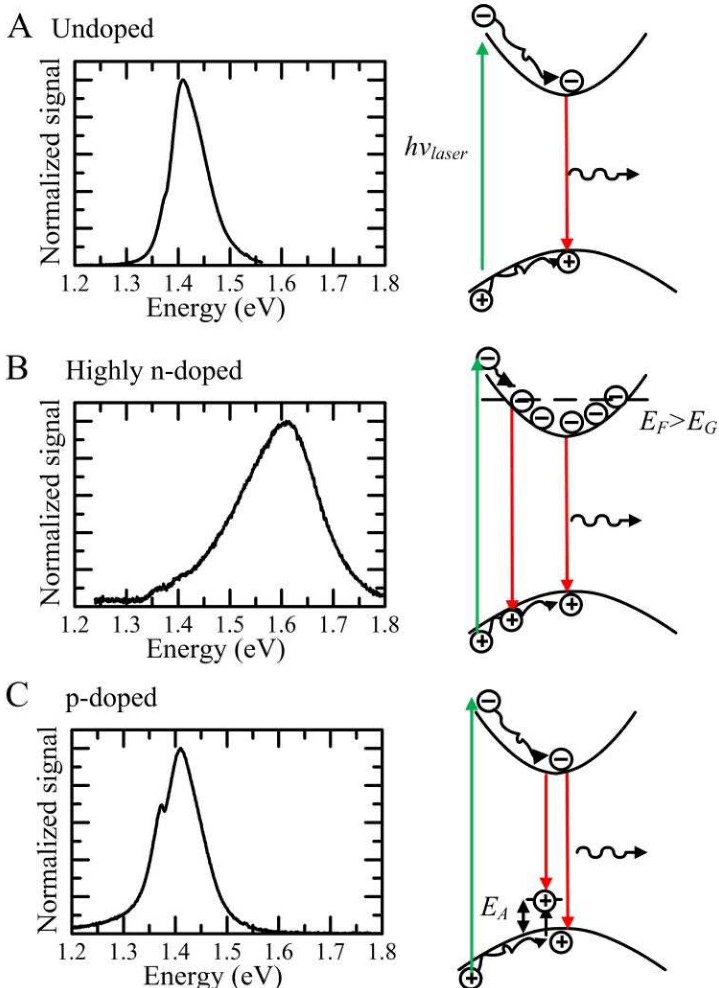

Figure 6.2 Room temperature photoluminescence measurements of InP NWs. *A) Undoped, B) Highly n-doped (S), C) p-doped (Zn). The NWs have wurtzite crystal structure, which has a room temperature bandgap of 1.42 eV [61, 130].*

For a highly n-doped semiconductor the free electrons fill the conduction band, which shifts the Fermi energy above the conduction band edge (Fig. 6.2 B). This leads to broadening and blue-shift in PL since all conduction band electrons can contribute to the PL signal, and is called Burstein-Moss shift [131, 132] (paper IV).

The amount of blueshift depends on the number of electrons and the density of states in the conduction band. In a simple parabolic-band model, the shift of the PL edge (E_F-E_C=ΔE), is given by:

$$\Delta E = \left(\frac{\hbar^2}{2m_{eff}}\right)(3\pi^2 n)^{2/3} \approx \frac{16.9}{m_{eff}}\left(\frac{n}{10^{19}cm^{-3}}\right)^{2/3} \text{(meV)} \quad (6.4)$$

Here, $\hbar$ is the reduced Planck's constant, m_{eff} the electron effective mass, and n the carrier concentration. Since the effective mass is usually a well-known material parameter, the carrier concentration can be directly determined from the PL spectrum.

The shift is larger for low effective mass, which makes this method more useful for low-bandgap materials. The shift is smaller for p-doped semiconductors, since the effective mass of holes is much higher than that of electrons. The binding energy of holes is also larger, typically around 40 meV in InP compared with 6 meV for electrons. On the other hand, this makes it possible to see acceptor states as distinct lines in PL (Fig. 6.2C).

There are other optical techniques which can be used to study doping of NWs, such as Raman spectroscopy [133] and terahertz photoconductivity measurements [134].

6.3 Electron beam and X-ray methods

In PL, photons with a slightly larger energy than the bandgap are used, that is, photons with an energy on the order of a few eV. Instead, electrons or high-energy photons (X-rays) can be used to excite the sample, and there are a large number of such techniques.

Energy dispersive x-ray spectroscopy (EDS) is a standard technique for characterization of NW heterostructures. The high-energy electrons, usually from a TEM, induce x-ray emission which has characteristic energy for each element. EDS detects dopant elements rather than carrier concentrations. This technique has high spatial resolution, but the relatively low sensitivity (typically a few tenths of percent) makes it difficult to use for doping. Nevertheless, it has recently been possible to detect Se in InAs NWs [107], Zn in InP NWs (paper II) as well as S in

H_2S-doped InP NWs (paper IV). In the latter case, the signal was strong enough to allow radial scans displaying increased signal at the surface of the NWs.

In photoemission electron microscopy (PEEM), electrons are emitted from the sample using UV or X-ray light. The emission depends on the carrier concentration, and this can be used for doping investigations [135].

6.4 Mass spectrometric methods

Secondary ion mass spectrometry (SIMS) is a standard technique for characterization of doping in thin film semiconductors. In this method the sample is sputtered by a focused (primary) ion beam, and the ejected (secondary) ions from the sample are collected and analyzed with mass spectrometry. It offers high sensitivity but it is a destructive method by design. The spatial resolution depends strongly on the details of the system used, but is generally far from the resolution of EDS. SIMS measures the dopant concentration rather than the carrier concentration. For instance, Lew et al. used SIMS for comparing different boron precursors for doping of Si NW [136]. Putnam et al. investigated the radial distribution of the Au content within Au-seeded large micrometer-diameter wires and set an upper limit of 1.7×10^{16} atoms/cm^3 [137].

Atom probe tomography (APT) is a development of SIMS where a needle-shaped sample is exposed to pulsed electrical fields which rip out ions by field emission. By time of flight measurements combined with an array mass spectrometer detector, a three-dimensional reconstruction of the probed sample can be created. The detection limit can be lower than 10^{18} atoms/cm^3 and the spatial resolution can be in the sub-nanometer range. In principle the original position of every ion detected - up to 50% of all ions which have been emitted - can be determined. Perea et al. pioneered the use of APT for NW characterization [138], and have later studied Au incorporation [139] and dopant incorporation [140] in NWs. The combination of low detection limits and high spatial resolution in some ways makes APT the ultimate tool for doping characterization, but there are limitations. The sample preparation is elaborate, the APT process is slow and only a part of the NW volume can be sampled.

6.5 Scanning probe methods

Various scanning probe techniques have been employed to investigate NW doping [141-143]. Scanning probe methods can have very high spatial resolution and are typically surface-sensitive. Similarly to optical techniques, qualitative indications of doping can often be found, but quantitative measurements are more challenging. The doping of Si NW was quantitatively studied by Allen et al. with scanning photocurrent microscopy (SPCM) [77]. Koren et al. used Kelvin probe force microscopy (KPFM) and successive etching steps to obtain the radial distribution of dopants in Si NWs [144], and they also combined KPFM with SPCM to investigate the axial doping profile of Si NWs [145]. Scanning spreading resistance microscopy (SSRM) has also been used to measure the conductivity of NWs standing as-grown [146] as well as in cross-section [147].

7 Conclusions

The results in this thesis demonstrate that III-V NWs can be successfully p- and n-doped, and that the doping can be used in devices such as solar cells and tunnel diodes. Several different materials have been investigated, in particular InP since it has a suitable bandgap for solar cells. In many cases, *in situ* doping gives strong effects on the growth rate and the crystal structure, as well as changes in the composition of ternary compounds.

There is a lack of detailed understanding of the incorporation of dopants, which is directly related to the difficulties in measuring the doping. Often the results are qualitative rather than quantitative, such as for p-doping of InP NWs. It is even more challenging to understand non-steady state phenomena, such as memory effects after switching off a dopant source.

The limited understanding of doping, however, does not prevent *in situ* doping from being successfully applied in devices. In this thesis two types of Esaki tunnel diodes have been demonstrated, which are arguably the most demanding device in terms of high doping and sharp transitions from p- to n-doping.

The overall purpose of this thesis has been to develop NW-based solar cells. In the last manuscript (X), promising single InP junction devices with 13.8% efficiency are demonstrated. The absorption is excellent despite only 12% surface coverage, against intuition but in line with theoretical predictions. The most surprising result is perhaps that a very high open-circuit voltage, exceeding that of the planar record device, can be achieved, despite the inherently high surface to volume ratios of nanostructured devices. Understanding this result will require more experimental investigations of for instance carrier lifetimes and surface passivation.

The next logical step in the development of NW-based solar cells is to make dual junction devices based on low-bandgap InP and high-bandgap GaInP diodes, which will require tunnel diodes in the right materials combination (n-InP to p-GaInP). A more thorough understanding of the dynamics of doping incorporation is needed, especially regarding transient phenomena as dopant sources are switched on or off, and new techniques for achieving sharp transitions should be explored.

References

[1] International Energy Agency, *2011 Key World Energy Statistics*. (IEA, 2011).

[2] H. Karttunen, P. Kröger, H. Oja, M. Poutanen, K. J. Donner, *Fundamental astronomy*. (Springer-Verlag, Berlin, 2nd ed., 1994).

[3] G. W. Crabtree, N. S. Lewis, *Solar Energy Conversion*. Physics Today, 2007, 60, 37

[4] Fraunhofer Institute for Solar Energy Systems, *Photvoltaics report 2012*. (FISE, 2012).

[5] European Photovoltaic Industry Association, *Global Market Outlook for Photovoltaics until 2016*. (EPIA, 2011).

[6] M. A. Green, K. Emery, Y. Hishikawa, W. Warta, E. D. Dunlop, *Solar cell efficiency tables (version 40)*. Progress in Photovoltaics: Research and Applications, 2012, 20, 606

[7] T. Mårtensson, C. P. T. Svensson, B. A. Wacaser, M. W. Larsson, W. Seifert, K. Deppert, A. Gustafsson, L. R. Wallenberg, L. Samuelson, *Epitaxial III-V nanowires on silicon*. Nano Letters, 2004, 4, 1987

[8] K. Tomioka, M. Yoshimura, T. Fukui, *A III-V nanowire channel on silicon for high-performance vertical transistors*. Nature, 2012, 488, 189

[9] M. T. Borgström, J. Wallentin, M. Heurlin, S. Fält, P. Wickert, J. Leene, M. H. Magnusson, K. Deppert, L. Samuelson, *Nanowires With Promise for Photovoltaics*. IEEE Journal of Selected Topics in Quantum Electronics, 2011, 17, 1050

[10] C. Colombo, M. Heibeta, M. Grätzel, A. Fontcuberta i Morral, *Gallium arsenide p-i-n radial structures for photovoltaic applications*. Applied Physics Letters, 2009, 94, 173108

[11] E. C. Garnett, M. L. Brongersma, Y. Cui, M. D. McGehee, *Nanowire Solar Cells*. Annual Review of Materials Research, Vol 41, 2011, 41, 269

[12] H. Goto, K. Nosaki, K. Tomioka, S. Hara, K. Hiruma, J. Motohisa, T. Fukui, *Growth of Core–Shell InP Nanowires for Photovoltaic Application by Selective-Area Metal Organic Vapor Phase Epitaxy*. Applied Physics Express, 2009, 2 (2009) 035004,

[13] J. F. Wang, M. S. Gudiksen, X. F. Duan, Y. Cui, C. M. Lieber, *Highly polarized photoluminescence and photodetection from single indium phosphide nanowires*. Science, 2001, 293, 1455

[14] A. Luque, S. Hegedus, Eds., *Handbook of PhotoVoltaic Science and Engineering*, (Wiley Chichester, 2003).

[15] W. Shockley, H. J. Queisser, *Detailed Balance Limit of Efficiency of P-N Junction Solar Cells*. Journal of Applied Physics, 1961, 32, 510

[16] C. H. Henry, *Limiting Efficiencies of Ideal Single and Multiple Energy-Gap Terrestrial Solar-Cells*. Journal of Applied Physics, 1980, 51, 4494

[17] S. L. Diedenhofen, G. Vecchi, R. E. Algra, A. Hartsuiker, O. L. Muskens, G. Immink, E. P. A. M. Bakkers, W. L. Vos, J. G. Rivas, *Broad-band and Omnidirectional Antireflection Coatings Based on Semiconductor Nanorods*. Advanced Materials, 2009, 21, 973

[18] R. R. King, D. C. Law, K. M. Edmondson, C. M. Fetzer, G. S. Kinsey, H. Yoon, R. A. Sherif, N. H. Karam, *40% efficient metamorphic GaInP/GaInAs/Ge multijunction solar cells*. Applied Physics Letters, 2007, 90, 183516

[19] L. Esaki, *New Phenomenon in Narrow Germanium p-n Junctions*. Physical Review, 1958, 109, 603

[20] S. M. Sze, K. K. Ng, *Physics of semiconductor devices*. (Wiley, New York, 3rd, 2007).

[21] J. F. Geisz, D. J. Friedman, *III–N–V semiconductors for solar photovoltaic applications*. Semiconductor Science and Technology, 2002, 17, 769

[22] Y.-J. Kim, J.-H. Lee, G.-C. Yi, *Vertically aligned ZnO nanostructures grown on graphene layers*. Applied Physics Letters, 2009, 95, 213101

[23] P. Caroff, M. E. Messing, B. M. Borg, K. A. Dick, K. Deppert, L. E. Wernersson, *InSb heterostructure nanowires: MOVPE growth under extreme lattice mismatch*. Nanotechnology, 2009, 20, 495606

[24] N. Anttu, H. Q. Xu, *Coupling of Light into Nanowire Arrays and Subsequent Absorption*. Journal of Nanoscience and Nanotechnology, 2010, 10, 7183

[25] X. F. Duan, Y. Huang, Y. Cui, J. F. Wang, C. M. Lieber, *Indium phosphide nanowires as building blocks for nanoscale electronic and optoelectronic devices*. Nature, 2001, 409, 66

[26] B. Dou, R. Jia, H. Li, C. Chen, W. Ding, Y. Meng, Z. Xing, X. Liu, T. Ye, *High performance radial p-n junction solar cell based on silicon nanopillar array with enhanced decoupling mechanism*. Applied Physics Letters, 2012, 101, 183901

[27] M. Heurlin, P. Wickert, S. Fält, M. T. Borgström, K. Deppert, L. Samuelson, M. H. Magnusson, *Axial InP Nanowire Tandem Junction Grown on a Silicon Substrate*. Nano Letters, 2011, 11, 2028

[28] T. J. Kempa, B. Z. Tian, D. R. Kim, J. S. Hu, X. L. Zheng, C. M. Lieber, *Single and Tandem Axial p-i-n Nanowire Photovoltaic Devices*. Nano Letters, 2008, 8, 3456

[29] L. Y. Cao, J. S. White, J. S. Park, J. A. Schuller, B. M. Clemens, M. L. Brongersma, *Engineering light absorption in semiconductor nanowire devices*. Nature Materials, 2009, 8, 643

[30] M. D. Kelzenberg, S. W. Boettcher, J. A. Petykiewicz, D. B. Turner-Evans, M. C. Putnam, E. L. Warren, J. M. Spurgeon, R. M. Briggs, N. S. Lewis, H. A. Atwater, *Enhanced absorption and carrier collection in Si wire arrays for photovoltaic applications (vol 9, pg 239, 2010)*. Nature Materials, 2010, 9, 368

[31] J. Kupec, R. L. Stoop, B. Witzigmann, *Light absorption and emission in nanowire array solar cells*. Optics Express, 2010, 18, 27589

[32] W. U. Huynh, J. J. Dittmer, A. P. Alivisatos, *Hybrid nanorod-polymer solar cells*. Science, 2002, 295, 2425

[33] J. Tang, Z. Huo, S. Brittman, H. Gao, P. Yang, *Solution-processed core-shell nanowires for efficient photovoltaic cells*. Nature Nanotechnology, 2011, 6, 568

[34] S. Jeong, S. Wang, Y. Cui, *Nanoscale photon management in silicon solar cells*. Journal of Vacuum Science & Technology A: Vacuum, Surfaces, and Films, 2012, 30, 060801

[35] L. J. Lauhon, M. S. Gudiksen, C. L. Wang, C. M. Lieber, *Epitaxial core-shell and core-multishell nanowire heterostructures*. Nature, 2002, 420, 57

[36] B. M. Kayes, H. A. Atwater, N. S. Lewis, *Comparison of the device physics principles of planar and radial p-n junction nanorod solar cells*. Journal of Applied Physics, 2005, 97, 114302

[37] A. Yella, H.-W. Lee, H. N. Tsao, C. Yi, A. K. Chandiran, M. K. Nazeeruddin, E. W.-G. Diau, C.-Y. Yeh, S. M. Zakeeruddin, M. Grätzel, *Porphyrin-Sensitized Solar Cells with Cobalt (II/III)–Based Redox Electrolyte Exceed 12 Percent Efficiency*. Science, 2011, 334, 629

[38] A. H. Ip, S. M. Thon, S. Hoogland, O. Voznyy, D. Zhitomirsky, R. Debnath, L. Levina, L. R. Rollny, G. H. Carey, A. Fischer, K. W. Kemp, I. J. Kramer, Z. Ning, A. J. Labelle, K. W. Chou, A. Amassian, E. H. Sargent, *Hybrid passivated colloidal quantum dot solids*. Nature Nanotechnology, 2012, 7, 577

[39] R. S. Wagner, Ellis, W.C., *Vapor-Liquid-Solid Mechanism of Single Crystal Growth (New method growth catalysis from impurity whisker epitaxial + large crystal SI E)*. Applied Physics Letters, 1964, 4, 89

[40] M. Heurlin, M. H. Magnusson, D. Lindgren, M. Ek, L. R. Wallenberg, K. Deppert, L. Samuelson, *Continuous gas-phase synthesis of nanowires with tunable properties*. Nature, 2012, 492, 90

[41] B. A. Wacaser, K. A. Dick, J. Johansson, M. T. Borgström, K. Deppert, L. Samuelson, *Preferential Interface Nucleation: An Expansion of the VLS Growth Mechanism for Nanowires*. Advanced Materials, 2009, 21, 153

[42] D. L. Smith, *Thin-film deposition: principles and practice*. (McGraw-Hill, 1995).

[43] F. Glas, J.-C. Harmand, G. Patriarche, *Why Does Wurtzite Form in Nanowires of III-V Zinc Blende Semiconductors?* Physical Review Letters, 2007, 99, 146101

[44] V. G. Dubrovskii, *Physical Consequences of the Equivalence of Conditions for the Steady-State Growth of Nanowires and the Nucleation on Triple Phase Line*. Technical Physics Letters, 2011, 37, 53

[45] J. Wallentin, M. Ek, L. R. Wallenberg, L. Samuelson, K. Deppert, M. T. Borgström, *Changes in Contact Angle of Seed Particle Correlated with Increased Zincblende Formation in Doped InP Nanowires*. Nano Letters, 2010, 10, 4807

[46] V. A. Nebol'sin, A. A. Shchetinin, *Role of surface energy in the vapor-liquid-solid growth of silicon*. Inorganic Materials, 2003, 39, 899

[47] N. V. Sibirev, M. A. Timofeeva, A. D. Bol'shakov, M. V. Nazarenko, V. G. Dubrovskii, *Surface energy and crystal structure of nanowhiskers of III-V semiconductor compounds*. Physics of the Solid State, 2010, 52, 1531

[48] K. C. Mills, Y. C. Su, *Review of surface tension data for metallic elements and alloys: Part 1 - Pure metals*. International Materials Reviews, 2006, 51, 329

[49] I. Egry, J. Brillo, *Surface Tension and Density of Liquid Metallic Alloys Measured by Electromagnetic Levitation*. Journal of Chemical and Engineering Data, 2009, 54, 2347

[50] V. G. Dubrovskii, N. V. Sibirev, J. C. Harmand, F. Glas, *Growth kinetics and crystal structure of semiconductor nanowires*. Physical Review B, 2008, 78, 235301

[51] M. T. Borgström, G. Immink, B. Ketelaars, R. Algra, E. P. A. M. Bakkers, *Synergetic nanowire growth*. Nature Nanotechnology, 2007, 2, 541

[52] B. J. Kim, J. Tersoff, S. Kodambaka, M. C. Reuter, E. A. Stach, F. M. Ross, *Kinetics of Individual Nucleation Events Observed in Nanoscale Vapor-Liquid-Solid Growth*. Science, 2008, 322, 1070

[53] C. A. Larsen, N. I. Buchan, G. B. Stringfellow, *Mass-Spectrometric Studies of Phosphine Pyrolysis and Omvpe Growth of Inp*. Journal of Crystal Growth, 1987, 85, 148

[54] M. A. Verheijen, G. Immink, T. de Smet, M. T. Borgström, E. P. A. M. Bakkers, *Growth kinetics of heterostructured GaP-GaAs nanowires*. Journal of the American Chemical Society, 2006, 128, 1353

[55] M. T. Borgström, J. Wallentin, J. Trägårdh, P. Ramvall, M. Ek, L. R. Wallenberg, L. Samuelson, K. Deppert, *In Situ Etching for Total Control Over Axial and Radial Nanowire Growth*. Nano Research, 2010, 3, 264

[56] M. T. Borgström, J. Wallentin, K. Kawaguchi, L. Samuelson, K. Deppert, *Dynamics of extremely anisotropic etching of InP nanowires by HCl*. Chemical Physics Letters, 2011, 502, 222

[57] K. Hiruma, M. Yazawa, T. Katsuyama, K. Ogawa, K. Haraguchi, M. Koguchi, H. Kakibayashi, *Growth and Optical-Properties of Nanometer-Scale Gaas and Inas Whiskers*. Journal of Applied Physics, 1995, 77, 447

[58] J. Johansson, L. S. Karlsson, C. P. T. Svensson, T. Mårtensson, B. A. Wacaser, K. Deppert, L. Samuelson, W. Seifert, *Structural properties of (111)B-oriented III-V nanowires*. Nature Materials, 2006, 5, 574

[59] P. Caroff, J. Bolinsson, J. Johansson, *Crystal Phases in III--V Nanowires: From Random Toward Engineered Polytypism*. IEEE Journal of selected topics in quantum electronics, 2010, PP, 18

[60] V. G. Dubrovskii, G. E. Cirlin, N. V. Sibirev, F. Jabeen, J. C. Harmand, P. Werner, *New mode of vapor-liquid-solid nanowire growth*. Nano Letters, 2011, 11, 1247

[61] A. Mishra, L. V. Titova, T. B. Hoang, H. E. Jackson, L. M. Smith, J. M. Yarrison-Rice, Y. Kim, H. J. Joyce, Q. Gao, H. H. Tan, C. Jagadish, *Polarization and temperature dependence of photoluminescence from zincblende and wurtzite InP nanowires*. Applied Physics Letters, 2007, 91, 263104

[62] M. Murayama, T. Nakayama, *Chemical Trend of Band Offsets at Wurtzite Zincblende Heterocrystalline Semiconductor Interfaces*. Physical Review B, 1994, 49, 4710

[63] M. Mattila, T. Hakkarainen, M. Mulot, H. Lipsanen, *Crystal-structure-dependent photoluminescence from InP nanowires*. Nanotechnology, 2006, 17, 1580

[64] L. Zhang, J.-W. Luo, A. Zunger, N. Akopian, V. Zwiller, J.-C. Harmand, *Wide InP Nanowires with Wurtzite/Zincblende Superlattice Segments Are Type-II whereas Narrower Nanowires Become Type-I: An Atomistic Pseudopotential Calculation*. Nano Letters, 2010, 10, 4055

[65] C. Thelander, P. Caroff, S. Plissard, A. W. Dey, K. A. Dick, *Effects of Crystal Phase Mixing on the Electrical Properties of InAs Nanowires*. Nano Letters, 2011, 11, 2424

[66] M. D. Schroer, J. R. Petta, *Correlating the Nanostructure and Electronic Properties of InAs Nanowires*. Nano Letters, 2010, 10, 1618

[67] T. Mårtensson, P. Carlberg, M. Borgström, L. Montelius, W. Seifert, L. Samuelson, *Nanowire arrays defined by nanoimprint lithography*. Nano Letters, 2004, 4, 699

[68] M. H. Magnusson, K. Deppert, J. O. Malm, J. O. Bovin, L. Samuelson, *Size-selected gold nanoparticles by aerosol technology*. Nanostructured Materials, 1999, 12, 45

[69] M. E. Messing, K. Hillerich, J. Bolinsson, K. Storm, J. Johansson, K. A. Dick, K. Deppert, *A comparative study of the effect of gold seed particle preparation method on nanowire growth*. Nano Research, 2010, 3, 506

[70] K. Kawaguchi, M. Heurlin, D. Lindgren, M. Borgström, M. Ek, L. Samuelson, *InAs quantum dots and quantum wells grown on stacking-fault controlled InP nanowires with wurtzite crystal structure*. Applied Physics Letters, 2011, 99, 131915

[71] K. Haraguchi, T. Katsuyama, K. Hiruma, K. Ogawa, *Gaas p-n-junction formed in quantum wire crystals*. Applied Physics Letters, 1992, 60, 745

[72] Y. Cui, X. F. Duan, J. T. Hu, C. M. Lieber, *Doping and electrical transport in silicon nanowires*. Journal of Physical Chemistry B, 2000, 104, 5213

[73] J. Dufouleur, C. Colombo, T. Garma, B. Ketterer, E. Uccelli, M. Nicotra, A. F. I. Morral, *P-Doping Mechanisms in Catalyst-Free Gallium Arsenide Nanowires*. Nano Letters, 2010, 10, 1734

[74] E. Kuphal, *Preparation and Characterization of LPE InP*. Journal of Crystal Growth, 1981, 54, 117

[75] G. B. Stringfellow, *The Role of Impurities in III/V Semiconductors Grown by Organometallic Vapor-Phase Epitaxy*. Journal of Crystal Growth, 1986, 75, 91

[76] B. Z. Tian, X. L. Zheng, T. J. Kempa, Y. Fang, N. F. Yu, G. H. Yu, J. L. Huang, C. M. Lieber, *Coaxial silicon nanowires as solar cells and nanoelectronic power sources*. Nature, 2007, 449, 885

[77] J. E. Allen, D. E. Perea, E. R. Hemesath, L. J. Lauhon, *Nonuniform Nanowire Doping Profiles Revealed by Quantitative Scanning Photocurrent Microscopy*. Advanced Materials, 2009, 21, 3067

[78] J. Wallentin, M. E. Messing, E. Trygg, L. Samuelson, K. Deppert, M. T. Borgström, *Growth of doped InAsyP1-y nanowires with InP shells*. Journal of Crystal Growth, 2011, 331, 8

[79] S. G. Ghalamestani, M. Heurlin, L.-E. Wernersson, S. Lehmann, K. A. Dick, *Growth of InAs/InP core–shell nanowires with various pure crystal structures*. Nanotechnology, 2012, 23, 285601

[80] R. Bhat, C. Caneau, C. E. Zah, M. A. Koza, W. A. Bonner, D. M. Hwang, S. A. Schwarz, S. G. Menocal, F. G. Favire, *Orientation dependence of S, Zn, Si, Te, and Sn doping in OMCVD growth of InP and GaAs: application to DH lasers and lateral p—n junction arrays grown on non-planar substrates*. Journal of Crystal Growth, 1991, 107, 772

[81] Y. Moon, S. Si, E. Yoon, S. J. Kim, *Low temperature photoluminescence characteristics of Zn-doped InP grown by metalorganic chemical vapor deposition*. Journal of Applied Physics, 1998, 83, 2261

[82] H. Peelaers, B. Partoens, F. M. Peeters, *Formation and segregation energies of B and P doped and BP codoped silicon nanowires*. Nano Letters, 2006, 6, 2781

[83] M. V. Fernandez-Serra, C. Adessi, X. Blase, *Surface segregation and backscattering in doped silicon nanowires*. Physical Review Letters, 2006, 96, 166805

[84] P. Xie, Y. J. Hu, Y. Fang, J. L. Huang, C. M. Lieber, *Diameter-dependent dopant location in silicon and germanium nanowires*. Proceedings of the National Academy of Sciences of the United States of America, 2009, 106, 15254

[85] M. Diarra, Y. M. Niquet, C. Delerue, G. Allan, *Ionization energy of donor and acceptor impurities in semiconductor nanowires: Importance of dielectric confinement*. Physical Review B, 2007, 75, 045301

[86] M. T. Björk, H. Schmid, J. Knoch, H. Riel, W. Riess, *Donor deactivation in silicon nanostructures*. Nature Nanotechnology, 2009, 4, 103

[87] Z. G. Chen, L. N. Cheng, G. Q. Lu, J. Zou, *Sulfur-doped gallium phosphide nanowires and their optoelectronic properties*. Nanotechnology, 2010, 21, 375701

[88] H. W. Seo, S. Y. Bae, J. Park, M. I. Kang, S. Kim, *Nitrogen-doped gallium phosphide nanowires*. Chemical Physics Letters, 2003, 378, 420

[89] H. G. Lee, H. C. Jeon, T. W. Kang, T. W. Kim, *Gallium arsenide crystalline nanorods grown by molecular-beam epitaxy*. Applied Physics Letters, 2001, 78, 3319

[90] M. Hilse, M. Ramsteiner, S. Breuer, L. Geelhaar, H. Riechert, *Incorporation of the dopants Si and Be into GaAs nanowires*. Applied Physics Letters, 2010, 96, 193104

[91] K. Tomioka, J. Motohisa, S. Hara, K. Hiruma, T. Fukui, *GaAs/AlGaAs Core Multishell Nanowire-Based Light-Emitting Diodes on Si*. Nano Letters, 2010, 10, 1639

[92] K. Haraguchi, T. Katsuyama, K. Hiruma, K. Ogawa, *GaAs p-n junction formed in quantum wire crystals*. Applied Physics Letters, 1992, 60, 745

[93] K. Sladek, V. Klinger, J. Wensorra, M. Akabori, H. Hardtdegen, D. Grutzmacher, *MOVPE of n-doped GaAs and modulation doped GaAs/AlGaAs nanowires*. Journal of Crystal Growth, 2010, 312, 635

[94] J. A. Czaban, D. A. Thompson, R. R. LaPierre, *GaAs Core-Shell Nanowires for Photovoltaic Applications*. Nano Letters, 2009, 9, 148

[95] J. Caram, C. Sandoval, M. Tirado, D. Comedi, J. Czaban, D. A. Thompson, R. R. LaPierre, *Electrical characteristics of core-shell p-n GaAs nanowire structures with Te as the n-dopant*. Nanotechnology, 2010, 21, 134007

[96] C. Gutsche, A. Lysov, I. Regolin, A. Brodt, L. Liborius, J. Frohleiks, W. Prost, F. J. Tegude, *Ohmic contacts to n-GaAs nanowires*. Journal of Applied Physics, 2011, 110,

[97] B. Ketterer, E. Mikheev, E. Uccelli, A. Fontcuberta i Morral, *Compensation mechanism in silicon-doped gallium arsenide nanowires*. Applied Physics Letters, 2010, 97, 223103

[98] C. Gutsche, I. Regolin, K. Blekker, A. Lysov, W. Prost, F. J. Tegude, *Controllable p-type doping of GaAs nanowires during vapor-liquid-solid growth*. Journal of Applied Physics, 2009, 105, 024305

[99] J. Wallentin, J. M. Persson, J. B. Wagner, L. Samuelson, K. Deppert, M. T. Borgström, *High-Performance Single Nanowire Tunnel Diodes*. Nano Letters, 2010, 10, 974

[100] L. Rigutti, A. D. Bugallo, M. Tchernycheva, G. Jacopin, F. H. Julien, G. Cirlin, G. Patriarche, D. Lucot, L. Travers, J. C. Harmand, *Si Incorporation in InP Nanowires Grown by Au-Assisted Molecular Beam Epitaxy*. Journal of Nanomaterials, 2009, 2009, 435451

[101] M. T. Borgström, E. Norberg, P. Wickert, H. A. Nilsson, J. Trägårdh, K. A. Dick, G. Statkute, P. Ramvall, K. Deppert, L. Samuelson, *Precursor evaluation for in situ InP nanowire doping*. Nanotechnology, 2008, 19, 445602

[102] M. H. M. van Weert, A. Helman, W. van den Einden, R. E. Algra, M. A. Verheijen, M. T. Borgström, G. Immink, J. J. Kelly, L. P. Kouwenhoven, E. P. A. M. Bakkers, *Zinc Incorporation via the Vapor-Liquid-Solid Mechanism into InP Nanowires*. Journal of the American Chemical Society, 2009, 131, 4578

[103] S. De Franceschi, J. A. van Dam, E. Bakkers, L. F. Feiner, L. Gurevich, L. P. Kouwenhoven, *Single-electron tunneling in InP nanowires*. Applied Physics Letters, 2003, 83, 344

[104] C. Liu, L. Dai, L. P. You, W. J. Xu, G. G. Qin, *Blueshift of electroluminescence from single n-InP nanowire/p-Si heterojunctions due to the Burstein-Moss effect*. Nanotechnology, 2008, 19, 465203

[105] M. H. M. van Weert, O. Wunnicke, A. L. Roest, T. J. Eijkemans, A. Yu Silov, J. E. M. Haverkort, G. W. t Hooft, E. P. A. M. Bakkers, *Large redshift in photoluminescence of p-doped InP nanowires induced by Fermi-level pinning*. Applied Physics Letters, 2006, 88, 043109

[106] R. E. Algra, M. A. Verheijen, M. T. Borgström, L.-F. Feiner, G. Immink, W. J. P. van Enckevort, E. Vlieg, E. P. A. M. Bakkers, *Twinning superlattices in indium phosphide nanowires*. Nature, 2008, 456, 369

[107] C. Thelander, K. A. Dick, M. T. Borgström, L. E. Fröberg, P. Caroff, H. A. Nilsson, L. Samuelson, *The electrical and structural properties of n-type InAs nanowires grown from metal-organic precursors*. Nanotechnology, 2010, 21, 205703

[108] G. Hesham, M. Philipp, S. Heinz, D. B. Cedric, R. Reto, S. Andreas, R. Charles, K. Siegfried, E. M. Kirsten, R. Heike, T. B. Mikael, *In situ doping of catalyst-free InAs nanowires*. Nanotechnology, 2012, 23, 505708

[109] B. S. Sorensen, M. Aagesen, C. B. Sorensen, P. E. Lindelof, K. L. Martinez, J. Nygard, *Ambipolar transistor behavior in p-doped InAs nanowires grown by molecular beam epitaxy*. Applied Physics Letters, 2008, 92, 012119

[110] J. Wallentin, M. T. Borgström, *Doping of semiconductor nanowires*. Journal of Materials Research, 2011, 26, 2142

[111] M. T. Björk, J. Knoch, H. Schmid, H. Riel, W. Riess, *Silicon nanowire tunneling field-effect transistors*. Applied Physics Letters, 2008, 92, 193504

[112] E. I. Givargizov, *Periodic Instability in Whisker Growth*. Journal of Crystal Growth, 1973, 20, 217

[113] L. A. Xu, Y. Su, Y. Q. Chen, H. H. Xiao, L. A. Zhu, Q. T. Zhou, S. Li, *Synthesis and characterization of indium-doped ZnO nanowires with periodical single-twin structures*. Journal of Physical Chemistry B, 2006, 110, 6637

[114] D. Jacobsson, J. M. Persson, D. Kriegner, T. Etzelstorfer, J. Wallentin, J. B. Wagner, J. Stangl, L. Samuelson, K. Deppert, M. T. Borgström, *Particle-assisted GaxIn1-xP nanowire growth for designed band gap structures*. Nanotechnology, 2012, 23, 245601

[115] C. Blomers, T. Grap, M. I. Lepsa, J. Moers, S. Trellenkamp, D. Grutzmacher, H. Luth, T. Schapers, *Hall effect measurements on InAs nanowires*. Applied Physics Letters, 2012, 101, 152106

[116] K. Storm, F. Halvardsson, M. Heurlin, D. Lindgren, A. Gustafsson, P. M. Wu, B. Monemar, L. Samuelson, *Spatially resolved Hall effect measurement in a single semiconductor nanowire*. Nature Nanotechnology, 2012, 7, 718

[117] P. M. Morse, H. Feshbach, *Methods of Theoretical Physics*. (McGraw-Hill, New York, 1953).

[118] K. Storm, G. Nylund, M. Borgström, J. Wallentin, C. Fasth, C. Thelander, L. Samuelson, *Gate-Induced Fermi Level Tuning in InP Nanowires at Efficiency Close to the Thermal Limit*. Nano Letters, 2011, 11, 1127

[119] H. T. Ng, J. Han, T. Yamada, P. Nguyen, Y. P. Chen, M. Meyyappan, *Single crystal nanowire vertical surround-gate field-effect transistor*. Nano Letters, 2004, 4, 1247

[120] O. Wunnicke, *Gate capacitance of back-gated nanowire field-effect transistors*. Applied Physics Letters, 2006, 89, 083102

[121] D. R. Khanal, J. Wu, *Gate coupling and charge distribution in nanowire field effect transistors*. Nano Letters, 2007, 7, 2778

[122] X. C. Jiang, Q. H. Xiong, S. Nam, F. Qian, Y. Li, C. M. Lieber, *InAs/InP radial nanowire heterostructures as high electron mobility devices*. Nano Letters, 2007, 7, 3214

[123] D. G. Ivey, P. Jian, L. Wan, R. Bruce, S. Eicher, C. Blaauw, *Pd/Zn/Pd/Au Ohmic Contacts to P-Type Inp*. Journal of Electronic Materials, 1991, 20, 237

[124] Y. Cui, Z. H. Zhong, D. L. Wang, W. U. Wang, C. M. Lieber, *High performance silicon nanowire field effect transistors*. Nano Letters, 2003, 3, 149

[125] G. F. Zheng, W. Lu, S. Jin, C. M. Lieber, *Synthesis and fabrication of high-performance n-type silicon nanowire transistors*. Advanced Materials, 2004, 16, 1890

[126] C. Thelander, M. T. Björk, M. W. Larsson, A. E. Hansen, L. R. Wallenberg, L. Samuelson, *Electron transport in InAs nanowires and heterostructure nanowire devices*. Solid State Communications, 2004, 131, 573

[127] G. M. Cohen, M. J. Rooks, J. O. Chu, S. E. Laux, P. M. Solomon, J. A. Ott, R. J. Miller, W. Haensch, *Nanowire metal-oxide-semiconductor field effect transistor with doped epitaxial contacts for source and drain*. Applied Physics Letters, 2007, 90,

[128] J. Wallentin, M. Ek, L. R. Wallenberg, L. Samuelson, M. T. Borgström, *Electron Trapping in InP Nanowire FETs with Stacking Faults*. Nano Letters, 2011, 12, 151

[129] O. Hayden, M. T. Björk, H. Schmid, H. Riel, U. Drechsler, S. F. Karg, E. Lortscher, W. Riess, *Fully depleted nanowire field-effect transistor in inversion mode*. Small, 2007, 3, 230

[130] G. Tuin, M. Borgström, J. Trägårdh, M. Ek, L. Wallenberg, L. Samuelson, M.-E. Pistol, *Valence band splitting in wurtzite InP nanowires observed by photoluminescence and photoluminescence excitation spectroscopy*. Nano Research, 2011, 4, 159

[131] M. Bugajski, W. Lewandowski, *Concentration-Dependent Absorption and Photoluminescence of N-Type Inp*. Journal of Applied Physics, 1985, 57, 521

[132] J. Wallentin, K. Mergenthaler, M. Ek, L. R. Wallenberg, L. Samuelson, K. Deppert, M. E. Pistol, M. T. Borgström, *Probing the Wurtzite Conduction Band Structure Using State Filling in Highly Doped InP Nanowires*. Nano Letters, 2011, 11, 2286

[133] T. Kawashima, G. Imamura, T. Saitoh, K. Komori, M. Fujii, S. Hayashi, *Raman scattering studies of electrically active impurities in in situ B-Doped silicon nanowires: Effects of annealing and oxidation*. Journal of Physical Chemistry C, 2007, 111, 15160

[134] P. Parkinson, H. J. Joyce, Q. Gao, H. H. Tan, X. Zhang, J. Zou, C. Jagadish, L. M. Herz, M. B. Johnston, *Carrier Lifetime and Mobility Enhancement in Nearly Defect-Free Core-Shell Nanowires Measured Using Time-Resolved Terahertz Spectroscopy*. Nano Letters, 2009, 9, 3349

[135] M. Hjort, J. Wallentin, R. Timm, A. A. Zakharov, J. N. Andersen, L. Samuelson, M. T. Borgström, A. Mikkelsen, *Doping profile of InP nanowires directly imaged by photoemission electron microscopy*. Applied Physics Letters, 2011, 99, 233113

[136] K. K. Lew, L. Pan, T. E. Bogart, S. M. Dilts, E. C. Dickey, J. M. Redwing, Y. F. Wang, M. Cabassi, T. S. Mayer, S. W. Novak, *Structural and electrical properties of trimethylboron-doped silicon nanowires*. Applied Physics Letters, 2004, 85, 3101

[137] M. C. Putnam, M. A. Filler, B. M. Kayes, M. D. Kelzenberg, Y. B. Guan, N. S. Lewis, J. M. Eiler, H. A. Atwater, *Secondary Ion Mass Spectrometry of Vapor-Liquid-Solid Grown, Au-Catalyzed, Si Wires*. Nano Letters, 2008, 8, 3109

[138] D. E. Perea, J. E. Allen, S. J. May, B. W. Wessels, D. N. Seidman, L. J. Lauhon, *Three-dimensional nanoscale composition mapping of semiconductor nanowires*. Nano Letters, 2006, 6, 181

[139] J. E. Allen, E. R. Hemesath, D. E. Perea, J. L. Lensch-Falk, Z. Y. Li, F. Yin, M. H. Gass, P. Wang, A. L. Bleloch, R. E. Palmer, L. J. Lauhon, *High-resolution detection of Au catalyst atoms in Si nanowires*. Nature Nanotechnology, 2008, 3, 168

[140] D. E. Perea, E. R. Hemesath, E. J. Schwalbach, J. L. Lensch-Falk, P. W. Voorhees, L. J. Lauhon, *Direct measurement of dopant distribution in an individual vapour-liquid-solid nanowire*. Nature Nanotechnology, 2009, 4, 315

[141] D. D. D. Ma, C. S. Lee, S. T. Lee, *Scanning tunneling microscopic study of boron-doped silicon nanowires*. Applied Physics Letters, 2001, 79, 2468

[142] C. Yang, Z. H. Zhong, C. M. Lieber, *Encoding electronic properties by synthesis of axial modulation-doped silicon nanowires*. Science, 2005, 310, 1304

[143] S. Vinaji, A. Lochthofen, W. Mertin, I. Regolin, C. Gutsche, W. Prost, F. J. Tegude, G. Bacher, *Material and doping transitions in single GaAs-based nanowires probed by Kelvin probe force microscopy*. Nanotechnology, 2009, 20, 385702

[144] E. Koren, N. Berkovitch, Y. Rosenwaks, *Measurement of Active Dopant Distribution and Diffusion in Individual Silicon Nanowires*. Nano Letters, 2010, 10, 1163

[145] E. Koren, Y. Rosenwaks, J. E. Allen, E. R. Hemesath, L. J. Lauhon, *Nonuniform doping distribution along silicon nanowires measured by Kelvin probe force microscopy and scanning photocurrent microscopy*. Applied Physics Letters, 2009, 95, 092105

[146] C. Celle, C. Mouchet, E. Rouviere, J. P. Simonato, D. Mariolle, N. Chevalier, A. Brioude, *Controlled in Situ n-Doping of Silicon Nanowires during VLS Growth and Their Characterization by Scanning Spreading Resistance Microscopy*. Journal of Physical Chemistry C, 2010, 114, 760

[147] X. Ou, P. Das Kanungo, R. Kögler, P. Werner, U. Gösele, W. Skorupa, X. Wang, *Carrier Profiling of Individual Si Nanowires by Scanning Spreading Resistance Microscopy*. Nano Letters, 2010, 10, 171

Acknowledgements

This section has been the hardest one to write. No man is an island, and I wouldn't have gotten this thesis done without help from many people. I would like to thank each and every one of you, but nevertheless, I would like to specifically mention a few people.

First, I would like to thank my three supervisors, who have all contributed greatly to this thesis. You have really complemented each other.

My main supervisor, Dr. Magnus Borgström, I thank of course for teaching me a great deal of science, in particular crystal growth. Thanks also for endless discussions around physics, kids and just about anything. It was a privilege to share room with you.

My two assistant, but highly experienced, supervisors, have also been very helpful. Prof. Knut Deppert has always had a kind word and two feet on the ground. From my first email five years ago, you have taken time for me. I have worked with quite a few managers, but no one nearly as inspiring as prof. Lars Samuelson. You see opportunities everywhere, with great excitement and curiosity.

Dr. Peter Ramvall, thank you for all the help with, and questions answered about, the epitaxy machines. Thanks also for numerous lunch conversations about everything from MFC calibration to child rearing.

Nicklas Anttu, the hardest working man in FTF, I've had a lot of fun working with you on the solar cells. Thank you for your patient responses on hundreds of emails and dozens of manuscript revisions.

Martin Ek, thanks for all the beautiful TEM work. Also, I appreciate your taste in jackets.

The solar cell development has been a real team effort, and it would not have been possible without a lot of work from the people at Sol Voltaics: Dr. Martin Magnusson, Damir Asoli, Dr. Maria Huffman, Dr. Ingvar Åberg, Peter Wickert, and a few others. It has been wonderful to work with such a friendly, professional and knowledgeable group of people. Thanks also to all the other colleagues from the AMON-RA project team.

Lund has arguably the world's highest density of nanowire growers, and I have learnt a great deal in discussions with fellow crystal growers: Dr. Sebastian Lehmann, Dr. Maria Messing, Karla Hillerich, Daniel Jacobsson, Magnus Heurlin, Alexander Berg, Dr. Mattias Borg, Dr. Kimberly Dick Thelander, Dr. Jonas Johansson, and many others. Thanks for making nanowire growth slightly less of a black magic, and thanks for all the good company inside and outside the lab.

The optical measurements have been an essential part of this thesis, although I wish I would have had more time for these. I'm very grateful for all the help I've gotten, both practical and theoretical, from Dr. Johanna Trägårdh, Kilian Mergenthaler, David Lindgren, Neimantas Vainorius, prof. Anders Gustafsson and Dr. Dan Hessman. A special thanks to prof. Mats-Erik Pistol for enlightening discussions about physics, Benoni, and many other things.

I would also like to acknowledge Dr. Claes Thelander, Kristian Storm, Gustav Nylund and Bahram Ganjipour for many interesting collaborations, and your patient help and support with device processing and electrical characterization. A number of dedicated diploma students have helped me as well: Erik Trygg, Laura Barrutia Poncela, and Andreas Jönsson.

Thanks to all the staff at the Lund Nano Lab, especially Dr. Ivan Maximov and Dr. Mariusz Graczyk, for lots of processing tips and for keeping the lab in such good shape. Thanks to Bengt Meuller and the other aerosol machine experts, for the deposition of 100 billion or so gold particles.

Thanks to the friendly people at Synchrotron Radiation Research: Prof. Anders Mikkelsen, Martin Hjort, and Dr. Rainer Timm, who never cease to come up with creative ways of studying nanowires. On that note, I would like to acknowledge the bio group for using my samples in the most unusual and interesting ways.

My family and I spent three wonderful months in Japan, during which I worked two months with Dr. Kenichi Kawaguchi at Fujitsu Laboratories, Ltd. You and your wife were extremely generous and helpful during our stay in Japan. Thank you for the help with the apartment and the furniture, the contracts and the bills, and the good company.

Thanks to my dear friends Simon and Christopher, to my parents Stefan and Gerd, and to my sister Frida, for all your support.

Sonja och Eskil, ni är världens snällaste och roligaste barn.

Last but certainly not least, thank you Verena. In the end, words fail me.